Life Sciences 268 (2021) 118936

Contents lists available at ScienceDirect

Life Sciences

journal homepage: www.elsevier.com/locate/lifescie

# Mitochondrial protective effects of PARP-inhibition in hypertension-induced myocardial remodeling and in stressed cardiomyocytes

K. Ordog [a,b], O. Horvath [a,b], K. Eros [b,c,d], K. Bruszt [a,b], Sz Toth [a], D. Kovacs [c], N. Kalman [c], B. Radnai [c], L. Deres [a,b,d], F. Gallyas Jr [b,c,d], K. Toth [a,b], R. Halmosi [a,b,*]

[a] 1st Department of Medicine, University of Pecs Medical School, Pecs, Hungary
[b] Szentagothai Research Centre, University of Pecs, Pecs, Hungary
[c] Department of Biochemistry and Medical Chemistry, University of Pecs Medical School, Pecs, Hungary
[d] HAS-UP Nuclear-Mitochondrial Interactions Research Group, Budapest, Hungary

ARTICLE INFO

*Keywords:*
Hypertension
Myocardial remodeling
Heart failure
Oxidative stress
PARP inhibition
Mitochondrial quality control

ABSTRACT

*Aims:* During oxidative stress mitochondria become the main source of endogenous reactive oxygen species (ROS) production. In the present study, we aimed to clarify the effects of pharmacological PARP-1 inhibition on mitochondrial function and quality control processes.

*Main methods:* L-2286, a quinazoline-derivative PARP inhibitor, protects against cardiovascular remodeling and heart failure by favorable modulation of signaling routes. We examined the effects of PARP-1 inhibition on mitochondrial quality control processes and function in vivo and in vitro. Spontaneously hypertensive rats (SHRs) were treated with L-2286 or placebo. In the in vitro model, 150 μM $H_2O_2$ stress was applied on neonatal rat cardiomyocytes (NRCM).

*Key findings:* PARP-inhibition prevented the development of left ventricular hypertrophy in SHRs. The interfibrillar mitochondrial network were less fragmented, the average mitochondrial size was bigger and showed higher cristae density compared to untreated SHRs. Dynamin related protein 1 (Drp1) translocation and therefore the fission of mitochondria was inhibited by L-2286 treatment. Moreover, L-2286 treatment increased the amount of fusion proteins (Opa1, Mfn2), thus preserving structural stability. PARP-inhibition also preserved the mitochondrial genome integrity. In addition, the mitochondrial biogenesis was also enhanced due to L-2286 treatment, leading to an overall increase in the ATP production and improvement in survival of stressed cells.

*Significance:* Our results suggest that the modulation of mitochondrial dynamics and biogenesis can be a promising therapeutical target in hypertension-induced myocardial remodeling and heart failure.

## 1. Introduction

Nowadays one of the most important cardiovascular risk factor is hypertension, by which approximately 30% of the adult population is affected globally [1]. Hypertension is associated with a significant risk of mortality and morbidity, because it can lead to coronary heart disease as well as to heart failure [2–4].

Manifest heart failure has still very poor prognosis despite the broadened therapeutical possibilities [4]. Therefore, the prevention of heart failure is essential. Although activation of the neurohumoral system plays an important role in the development of myocardial remodeling, the intrinsic myocardial changes are of great importance, too. In cardiomyocytes of chronically stressed heart (e.g. hypertension), there is a lack in high-energy phosphates and simultaneously an increased reactive oxygen species production (ROS). Both the low energy supply and the oxidative stress as a consequence of mitochondrial dysfunction play an important role in the development of hypertensive heart disease and its progression to heart failure [5,6].

Mitochondria are the predominant source of energy in cardiomyocytes, however, under pathological conditions such as hypertension or heart failure they become the main source of endogenous ROS production, too [5,7,8]. Free radicals can cause wide variety of damages

* Corresponding author at: 1st Department of Medicine, University of Pecs Medical School, Ifjusag str. 13, 7624 Pecs, Hungary.
*E-mail address:* halmosi.robert@pte.hu (R. Halmosi).

https://doi.org/10.1016/j.lfs.2020.118936
Received 2 September 2020; Received in revised form 27 November 2020; Accepted 12 December 2020
Available online 6 January 2021

in the cells, e.g. single-strand DNA breaks, what activates poly(ADP-ribose) polymerase (PARP) enzymes. Activated PARP enzyme binds ADP-ribose polymers to the damaged DNA region, by cleaving $NAD^+$ [9–13]. If the PARP enzyme is overactivated, the cellular $NAD^+$ stores are depleted, leading to a severe energy deficiency that causes programmed or necrotic cell death [13,14]. $H_2O_2$ is considered as a relevant source of ROS in cells because it can yield in the production of hydroxyl radicals and therefore can cause oxidative cell injury by compromising the mitochondrial function and structure [15]. Hydrogen peroxide is a small and stable molecule which can easily pass through the membranes and induces oxidative injury in the cells, therefore it is the most common way for modeling oxidative stress situations in vitro [16,17].

Previously we have demonstrated that pharmacological PARP-inhibition protects against the development of postinfarction-, hypertension-induced and toxic heart failure, as well as against hypertension-induced early cardiovascular damages (also known as hypertensive heart disease). Besides the orthodox effect of PARP-inhibition on $NAD^+$ preservation this protective effect was caused by favorable alterations of signaling routes [18–26]. In the present study, we aimed to clarify the effects of pharmacological PARP-1 inhibition on mitochondrial quality control processes and function.

## 2. Materials and methods

### 2.1. Materials

All chemicals for cell culture studies were purchased from Thermo Fisher Scientific and Gibco (Life Technologies, Carlsbad, CA, USA). Protease and phosphatase inhibitor cocktails and hydrogen peroxide were obtained from Sigma Aldrich Co. (St. Louis, MO, USA), NP-40 lysis buffer was purchased from Amresco (VWR International, Radnor, PA, USA). L-2286 was a gift of the Department of Organic and Pharmacological Chemistry, University of Pecs Medical School. MitoTracker Red CMXRos fluorescent dye was bought from Molecular Probes (Life Technologies, Carlsbad, CA, USA), JC-1 was obtained from Enzo Life Sciences (Enzo Biochem Inc., Farmingdale, NY, USA). The primary antibodies were purchased from Cell Signaling Technologies (Danvers, MA, USA), Novus Biologicals (Bio-Techne, Minneapolis, MN, USA), Abcam (Cambridge, UK), and Thermo Fisher Scientific (Life Technologies, Carlsbad, CA, USA). The horseradish peroxidase-conjugated anti-rabbit and anti-mouse IgG were obtained from Sigma-Aldrich Co. (St. Louis, MO, USA), XFp Cell Mito Stress Test Kit, XF Calibrant and XF Base Medium, Brilliant II QPCR Master Mix and PfuUltra II Hotstart PCR Master Mix were obtained from Agilent Technologies (Santa Clara, CA, USA). The primers for PCR reactions were purchased from Bio-Science Ltd. (Budapest, Hungary). EvaGreen™ dye was obtained from Biotium (Biotium, Hayward, CA, USA). All reagents were of the highest purity commercially available.

### 2.2. Ethics statement

The investigation conforms to the Guide for the Care and Use of Laboratory Animals published by the U.S. National Institutes of Health and was approved by the Animal Research Review Committee of the University of Pecs, Medical School (BA02/2000-2/2010).

### 2.3. Animal model and experimental protocol

10-week-old male spontaneously hypertensive (SHR) and Wistar Kyoto rats (WKY) were purchased from Charles River Laboratories (Wilmington, MA, USA) and were kept as we published earlier [24]. SHR rats were randomized into two groups: one group received no treatment (SHR-C, $n = 8$), whereas the other group (SHR-L, $n = 8$) received 5 mg/kg/day L-2286, a water-soluble PARP-inhibitor for 32 weeks. The third was an age-matched normotensive control group (WKY, $n = 8$). L-2286 was dissolved in the drinking water based on preliminary data about the volume of daily fluid consumption. Rats were inspected weekly to measure their weight as well as to observe their normal activity, respiration, responsiveness to manipulations and general aspects. At the end of the study animals were euthanized with an overdose of ketamine hydrochloride intraperitoneally and heparinized with sodium heparin (100 IU/rat i.p., Biochemie GmbH, Kundl, Austria).

### 2.4. Non-invasive evaluation of cardiac functions and dimensions

All animals were examined by echocardiography to exclude rats with any heart abnormalities. Transthoracic two-dimensional echocardiography was performed under inhalation anesthesia. Rats were lightly anesthetized with a mixture of 1.5% isoflurane (Forane, Abbott Laboratories, Hungary) and 98.5% oxygen. The chest of animals was shaved, acoustic coupling gel was applied, and warming pad was used to maintain normothermia. Cardiac dimensions and functions were measured from short- and long-axis views at the mid-papillary level by VEVO 770 high-resolution ultrasound imaging system (VisualSonics, Toronto, Canada) equipped with a 25 MHz transducer. Ejection fraction (EF), LV end-diastolic volume (LVEDV), LV end-systolic volume (LVESV), and the thickness of septum and posterior wall were determined.

### 2.5. Non-invasive blood pressure measurement

Blood pressure measurement were performed on each animal on two occasions at week 0 and 32 of the treatment period. Blood pressure measurement were performed by a non-invasive tail-cuff method by Hatteras SC1000 Blood Pressure Analysis System with rat species platform (Panlab, Harvard Apparatus; LE5001).

### 2.6. Determination of plasma B-type natriuretic peptide

After the sacrifice, blood samples were collected into Lavender Vacutainer tubes containing EDTA and aprotinin (0.6 IU/mL of blood) and were centrifuged at 1600*g* for 15 min at 4 °C to separate the plasma. Supernatants were collected and BNP-45 were determined by ELISA method as the manufacturer proposed (BNP-45, Rat ELISA Kit, Abcam, Cambridge, UK).

### 2.7. Electron microscopic examination of hearts

For electron microscopic analysis, hearts were perfused retrogradely through the aortic root with ice-cold PBS to wash away blood and then washed by modified Kranovsky fixative (2% paraformaldehyde, 2.5% glutaraldehyde, 0.1 M Na-cacodylate buffer, pH 7.4 and 3 mM $CaCl_2$). The electron microscopic samples were prepared as described earlier [27], and they were examined with a JEOL 1200EX-II electron microscope. Four animals of each group, 3–5 block from each animal were used. The area of interfibrillar mitochondria (IFM) were measured by free hand polygon selection ($n \sim 500$/group) using the NIH ImageJ software, where length of longitudinal axes and numbers of mitochondrial cristae were also evaluated.

### 2.8. Western blot analysis

The preparation of total Western blot samples from cardiac tissue were performed as described earlier [27]. Fractionated western blot sample preparation from cardiac tissue was performed using ice-cold isolation solution (150 mM NaCl, 5 mM TRIS, 1 mM EDTA, protease inhibitor 1:100, phosphatase inhibitor 1:100). Heart tissue was minced, samples were disrupted on ice with Turrax and then with Potter-Elvehjem tissue homogenizer. Samples were centrifuged for 12 min at 750*g*, then the supernatant, which was containing the cytosolic and mitochondrial fraction, was aspirated, the precipitated nucleus fraction was discarded. The supernatant was centrifuged for 12 min at 11,000*g*.

**Table 1**
Effect of L-2286 on echocardiographic parameters and on BNP level. WKY: 42-weeks-old normotensive age-matched animals, $n = 8$; SHR-C: 42-weeks old non-treated spontaneously hypertensive (SHR) rats, n = 8; SHR-L: 42-weeks-old SHR rats received L-2286 for 32 weeks, $n = 8$. EF: ejection fraction, LVEDV: left ventricular end-diastolic volume, LVESV: left ventricular end-systolic volume. Septum: thickness of septum, PW: thickness of posterior wall, SBP: systolic blood pressure, HR: heart rate, VW/BW: ventricular weight to body weight ratio. Values are mean ± SEM. [a] $p < 0.01$ vs. WKY, [b] $p < 0.05$ vs. SHR-C.

| | WKY | SHR-C | SHR-L |
|---|---|---|---|
| EF (%) | 70.24 ± 1.12 | 67.21 ± 1.22 | 69.13 ± 1.84 |
| LVEDV | 280.78 ± 9.93 | 350.78 ± 11.02[a] | 329.67 ± 12.53[a,b] |
| LVESV | 82.95 ± 2.48 | 115.11 ± 5.96[a] | 101.32 ± 3.34[a,b] |
| Septum | 1.43 ± 0.03 | 1.99 ± 0.03[a] | 1.72 ± 0.04[a,b] |
| PW | 1.45 ± 0.02 | 2.05 ± 0.02[a] | 1.74 ± 0.03[a,b] |
| LV weight (calc.) | 978 ± 17 | 1393 ± 13[a] | 1168 ± 45[a,b] |
| $SBP^{10w}$ (Hgmm) | 130 ± 5.4 | 182 ± 5.6[a] | 178 ± 3.6[a] |
| $SBP^{42w}$ (Hgmm) | 128 ± 4.8 | 231 ± 6.3[a] | 225 ± 2.4[a] |
| HR (beats $min^{-1}$) | 308 ± 13 | 339 ± 7.8 | 335 ± 9.2 |
| $VW/BW^{42w}$ (mg/g) | 3.01 ± 0.16 | 3.97 ± 0.22[a] | 3.38 ± 0.3[a,b] |
| Lung wet weight/dry $weight^{42w}$ | 4.74 ± 0.11 | 4.92 ± 0.24 | 4.87 ± 0.21 |
| BNP (ng/mL) | 2.06 ± 0.15 | 2.35 ± 0.03 | 2.23 ± 0.13 |

To gain the cytosolic fraction in the supernatant and mitochondrial in the precipitate, samples were harvested separately in 2× SDS–polyacrylamide gel electrophoresis sample buffer and denatured at 95 °C for 5 min. Electrophoresis and transfer of proteins were performed as described earlier [24]. Membranes were probed overnight at 4 °C with antibodies recognizing the following antigens: dynamin-related protein 1 (Drp1) (1:1000), optic atrophy 1 (Opa1, 1:1000), anti poly(ADP-ribose) (anti-PAR, 1:5000). Glyceraldehyde 3-phosphate dehydrogenase (GAPDH, for whole cell and cytoplasmic fraction) and pyruvate dehydrogenase complex (PDC, for mitochondrial fraction) were used as loading controls. Antibodies were purchased from Cell Signaling Technology, except for anti-PAR, from Alexis Biotechnology (London, UK). After scanning, results were quantified by the NIH Image J program. Densities of bands were normalized to the respective loading controls.

### 2.9. Neonatal rat cardiomyocyte (NRCM) cell culture

Cardiomyocytes were isolated from 1 to 3 days old neonatal Wistar rats using the Pierce™ Primary Cardiomyocyte Isolation Kit (Life Technologies, Carlsbad, CA, USA) following the manufacturer's instructions. The animals were sacrificed and then their hearts were removed and minced into 1–3 $mm^3$ pieces. The pieces were digested with an enzyme complex (Cardiomyocyte Isolation Enzyme 1 (with papain) and Cardiomyocyte Isolation Enzyme 2 (with thermolysin)). Purified NRCM cells were maintained in a humidified 5% $CO_2$ atmosphere at 37 °C, cells were cultured in specific Dulbecco's modified Eagle Medium (DMEM) for Primary Cell Isolation containing 10% fetal bovine serum (FBS) and antibiotic solution (1% penicillin and streptomycin solution).

### 2.10. Evaluation of the mitochondrial fragmentation

NRCM cells were seeded at a density of $10^5$ cells/well in 6-well plates on glass coverslips with gelatin coating and cultured for at least 2 days before experiment. On the day of experiment, cells were washed once with PBS and fresh medium was added, then cells were treated with $H_2O_2$ with or without L-2286. Group of cells: Control: cells without any treatment, Control+L-2286: cells incubated with 10 μM L-2286 for 0.5 h, $H_2O_2$: cells stressed with 150 μM $H_2O_2$ for 0.5 h, $H_2O_2$ + L-2286: cells stressed with 150 μM $H_2O_2$ and treated with 10 μM L-2286 for 0.5 h. After the appropriate treatment coverslips were rinsed in PBS and were added 300 nM MitoTracker Red CMXRos dissolved in PBS and incubated for 30 min at 37 °C. After incubation, coverslips were rinsed in PBS then imaged with a Nikon Eclipse Ti-U fluorescent microscope equipped with a Spot RT3 camera using a 60× objective and epifluorescent illumination.

### 2.11. Immunoblot analysis

NRCM cells were seeded into a 6-well plate and cultured. After the appropriate treatment, cells were harvested, the cell pellet was suspended in ice-cold PBS buffer, then centrifuged for 5 min at room temperature at 1200 rpm. The pellets were suspended in 300 μL NP-40 lysis buffer (Amresco, J619) containing protease and phosphatase inhibitor cocktail (1:100). The samples were shaken for 30 min at 4 °C and then centrifuged for 20 min (4 °C, 12,000 rpm). To each sample, 4× concentrated sodium dodecyl sulphate (SDS)-polyacrylamide gel electrophoresis sample buffer was added. Proteins were separated on a 10% SDS-polyacrylamide gel and transferred to nitrocellulose membranes. After blocking (1 h with 5% non-fat dry milk in Tris-buffered saline), membranes were probed overnight at 4 °C with primary antibody. We used the following antibodies and dilutions: anti-GAPDH (Cell Signaling Technologies 2118L, 1:1000), anti-Drp1 (Cell Signaling Technologies, 8570S, 1:1000), anti-phospho-$Drp1^{S616}$ (Cell Signaling Technologies, 12282S, 1:500), anti-phospho-$Drp1^{S637}$ (Cell Signaling Technologies, 4867S, 1:500), anti-mitofusin1 (Mfn1, Abcam, ab57602, 1:1000), anti-mitofusin2 (Mfn2, Cell Signaling Technologies, 9482S, 1:1000), anti-Opa1 (Cell Signaling Technologies, 80471S, 1:1000), anti-mitochondrial fission protein 1 (TTC11/Fis1, Abcam, ab71498, 2 μg/mL), anti-PDC (Thermo Fisher Scientific, PA5–66472, 1:1000), anti-peroxisome proliferator-activated receptor gamma coactivator 1-alpha (PGC1α, Novus Biologicals, NBP1-04676, 1:1000), anti-cAMP response element-binding protein (CREB, Cell Signaling Technologies, 4820S, 1:1000), anti-phospho-$CREB^{Ser133}$ (Cell Signaling Technologies, 9198S, 1:1000), anti-voltage dependent anion channel (VDAC, Cell Signaling Technologies, 4661S, 1:1000), anti-NADH dehydrogenase Fe-S protein 1 (NDUFs1, Novus Biologicals, NBP1-31142, 1:1000), anti-Ubiquinol-cytochrome *c* reductase core protein I (UQCRC1, Novus Biologicals, NBP2-03825, 1:1000), anti-Microtubule-associated protein 1 light chain 3 alpha (LC3A, Novus Biologicals, NB100-2331, 1:1000), anti-Poly (ADP-ribose) polymerase (PARP, Cell Signaling Technologies, 9532S, 1:1000). Membranes were washed 6-times for 5 min in Tris-buffered saline containing 0.1% Tween-20 before addition of appropriate horseradish peroxidase-conjugated secondary antibody (goat anti-rabbit IgG, Sigma Aldrich Co. A0545, 1:3000 dilution; rabbit anti-mouse IgG, Sigma Aldrich Co., A9044, 1:5000 dilution). Membranes were washed again as before, and then antibody-antigen complexes were visualized by enhanced chemiluminescence. The results of western blots were quantified by the ImageJ software (NIH, Bethesda, MD, USA). Each experiment was repeated three times with similar results.

### 2.12. Capillary Western immunoassay (Protein Simple Wes)

Capillary Western immunoassay was performed on a Protein Simple Wes system according to the manufacturer's instructions using a 12–240 kDa Separation Module (Bio-Techne R&D Systems, SM-W004) and the Anti-Rabbit Detection Module (DM-001). Fractionated NRCM samples were made as described in Section 2.5. NRCM samples were diluted to an appropriate concentration (0.3 mg/mL) in the sample buffer (100× diluted '10x Sample Buffer 2' from the Separation Module), then mixed with prepared Fluorescent Master Mix and heated at 95 °C for 5 min. The ladder, the samples, blocking reagent, primary and HRP-conjugated secondary antibodies, and the luminol-peroxide mixture as chemiluminescent substrate were pipetted into the plate. Instrument default settings were used: stacking and separation at 475 V for 30 min; blocking reagent for 5 min; primary and secondary antibody both for 30 min; Luminol/peroxide chemiluminescence detection were used in high dynamic range function. Compass software was used to

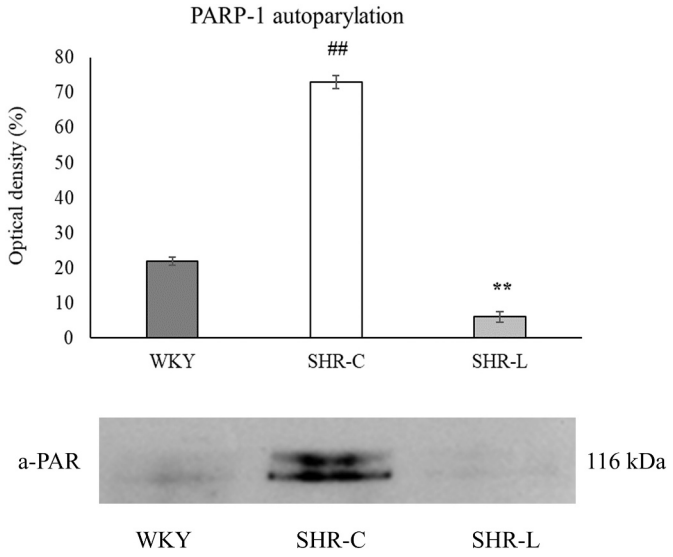


**Fig. 1.** The effect of L-2286 treatment on the auto-PARylation of PARP-1 enzyme. Representative Western-blot analysis and densitometric evaluation is shown. WKY: normotensive age-matched animals, SHR-C: non-treated spontaneously hypertensive (SHR) rats, SHR-L: SHR rats treated by 5 mg/kg/day L-2286 for 32 weeks. Values are means ± S.E.M, ($n = 4$). $^{\#\#}p < 0.01$ vs WKY, **p < 0.01 vs SHR-C.

process and analyze all data results.

### 2.13. JC-1 assay for mitochondrial membrane potential measurement

The mitochondrial membrane potential (ΔΨm) was measured using the mitochondrial membrane potential specific fluorescent probe, JC-1 (Enzo Life Sciences, ENZ-52304). The procedure is based on tracking the fluorescence shift from red to green, the J-aggregates located in mitochondrial matrix and converted to J-monomers while translocated through the mitochondrial permeability transition pore into the cytosol. NRCM cells were seeded onto glass coverslips coated with gelatin and cultured at least 2 days before the experiment. After treatment, cells were washed in PBS and then incubated for 15 min at 37 °C in media containing 2 μg/mL JC-1. The dye emits green fluorescence (530 nm) at low ΔΨm and red (590 nm) at high ΔΨm. Following incubation, the cells were washed once with PBS and then imaged with a Nikon Eclipse Ti-U fluorescent microscope equipped with a Spot RT3 camera using a 60× objective and epifluorescent illumination. All experiments were repeated three times. Fluorescent signals were quantified by using the ImageJ software (NIH, Bethesda, MD, USA).

### 2.14. Determination of mitochondrial oxygen consumption rate

Agilent Seahorse XFp Analyzer (Santa Clara, CA, USA) was used to determine the NRCM cells' oxygen consumption rate (OCR). Cell Mito Stress Kit is capable of real-time monitoring of mitochondrial oxygen consumption by examining the mitochondrial respiratory chain

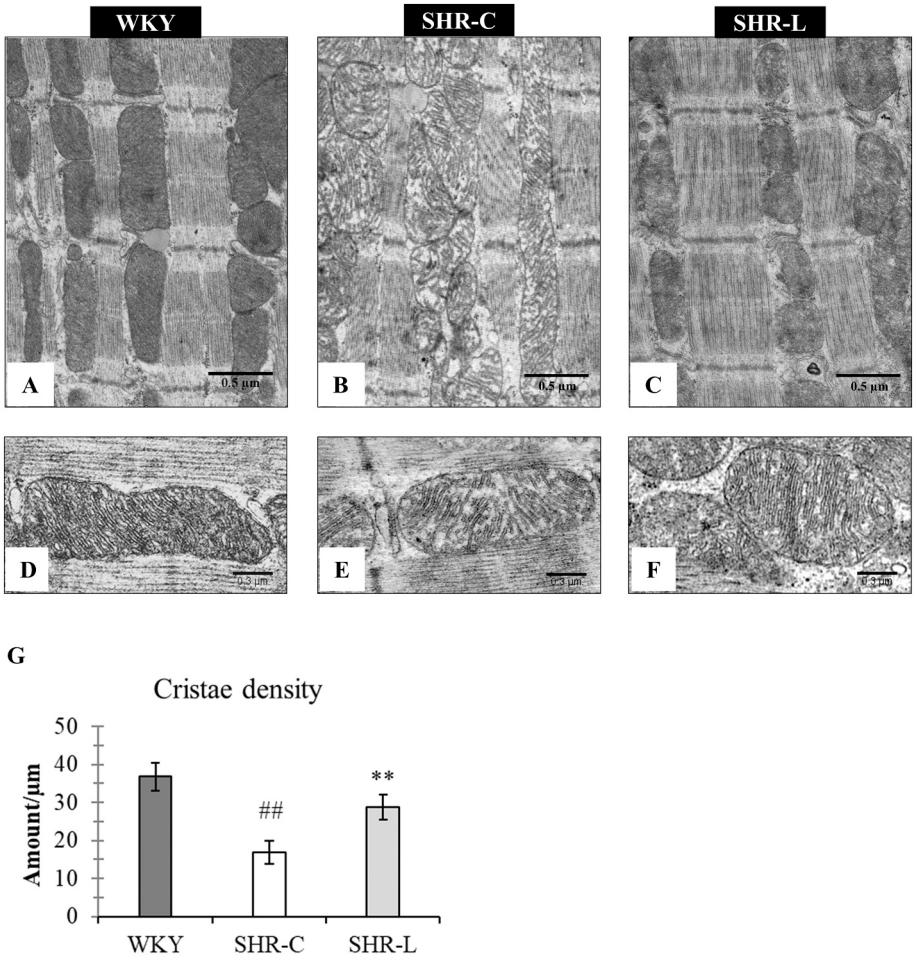





**Fig. 2.** Effect of PARP inhibition on the structure of interfibrillar mitochondria. (A-C) Representative electron micrographs of interfibrillar mitochondria in the myocardium of (A) WKY, (B) SHR-C and (C) SHR-L animals (magnification: 10 k, scale bar: 0.5 μm). (D-F) Ultrastructure of interfibrillar mitochondria in the myocardium of (D) WKY, (E) SHR-C and (F) SHR-L animals (magnification: 40 k, scale bar: 0.3 μm). (G) Mitochondrial cristae density. SHR-C: non-treated spontaneously hypertensive (SHR) rats, SHR-L: SHR rats treated by 5 mg/kg/day L-2286 for 32 weeks. Data are presented as mean ± S.E.M. $^{\#\#}p < 0.01$ vs. WKY, **p < 0.01 vs. SHR-C.

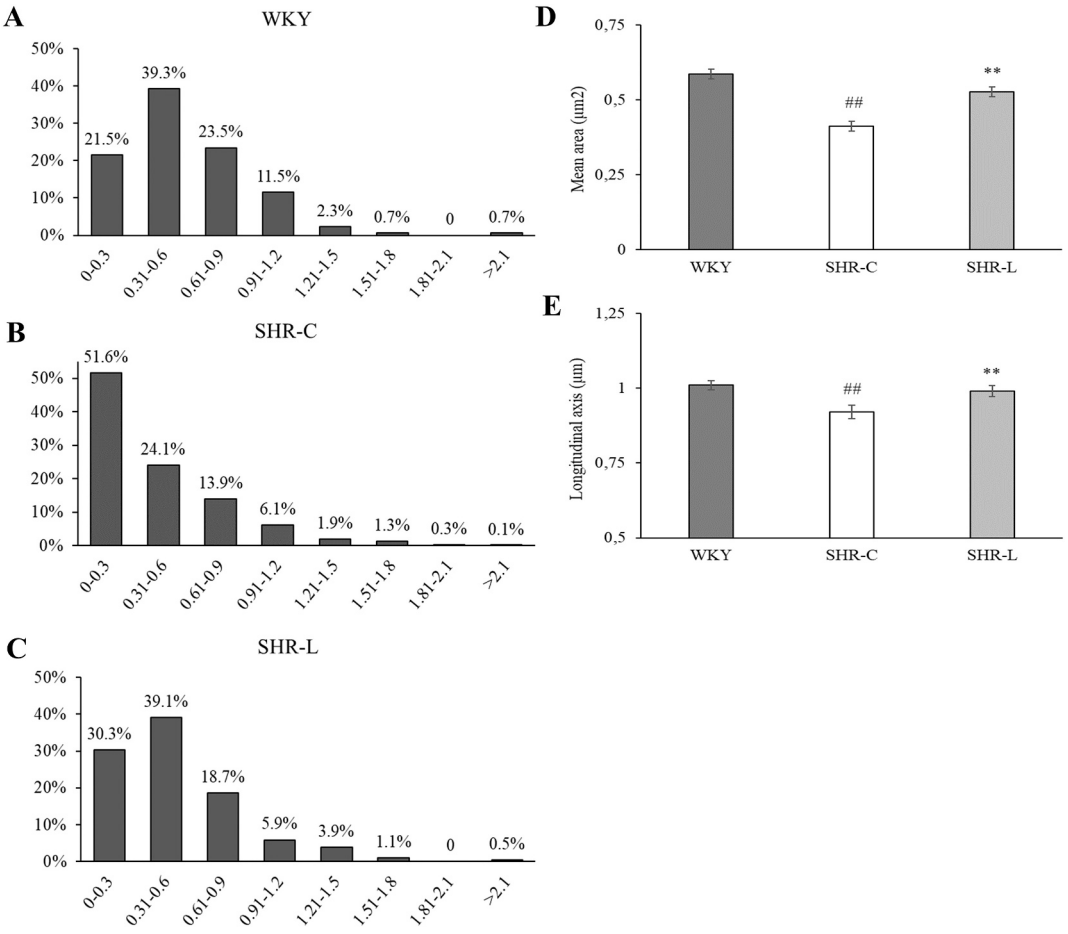


**Fig. 3.** Hypertension related fragmentation of interfibrillar mitochondria in the myocardium. Distribution of mitochondria based on their size in various area range groups: (A) WKY: normotensive age-matched animals, (B) SHR-C: non-treated spontaneously hypertensive (SHR) rats, (C) SHR-L: SHR rats treated by L-2286. (D) Mean mitochondrial area (E) Longitudinal axis of mitochondria. Values are means ± S.E.M. $^{**}p < 0.01$ vs. SHR-C, $^{\#\#}p < 0.01$ vs. WKY.

complexes. NRCM cells were seeded in XFp Miniplate at the density of $10^5$ cells/well in 80 µL complete growth medium (DMEM for Primary Cell Isolation containing 10% FBS and 1% antibiotic solution) and incubated at 37 °C, 5% $CO_2$ for 2 days. On the day before the assay, the XFp Sensor Cartridge was hydrated in XF Calibrant in non- $CO_2$ incubator at 37 °C overnight. On the day of the assay, after subjecting cells to the appropriate treatment, complete growth medium was removed and replaced with assay medium supplemented with 1 mM pyruvate, 2 mM glutamine, 10 mM glucose, pH 7.4. Before measurement oligomycin, FCCP and rotenone/antimycin A were loaded in the injection ports of the sensor cartridge. These compounds' final concentration was 1 µM and three measurements were taken after each injection.

### *2.15. Quantification of mitochondrial DNA (mtDNA) damage and relative mitochondrial DNA content by real-time PCR*

NRCM cells were used as the source of DNA for all experiments, and cells were grown in special DMEM with 10% FBS. After the appropriate treatment total DNA was isolated using GenElute™ Mammalian Genomic DNA Miniprep kit (Sigma Aldrich Co., St. Louis, MO, USA, G1N70). The following rat primer sequences were used: LRPCR (14,958 bp) forward: 5′-ATTTTCTCCCAGTTACGAAAG-3′, reverse: 5′-CTTGGTAAGTAAATTTCTTTCTCC-3′; SRPCR (210 bp) forward: 5′-ATGCACGATAGCTAAGACCCAA-3′; reverse: 5′-GCTGAATTAGCGAGAAGGGGTA-3′ [28]. The primer set for the short-range PCR (SRPCR) was located within the 12S rRNA region. Real-time DNA amplification was performed using a Bio Rad CFX96 Touch Real-Time PCR Detection System. Short fragment, cytochrome *c* oxidase subunit 1 (COX1), cytochrome *c* oxidase subunit 3 (COX3) and β-actin were done using a Brilliant QPCR Master Mix, while LRPCR was done using PfuUltra™ II Fusion HS DNA Polymerase. The final SRPCR, COX1, COX3 and β-actin cycling parameters were: 10 min at 95 °C followed by 30 s at 95 °C, 1 min at 60 °C, 30 s at 72 °C for 40 cycles. The final LRPCR cycling parameters were: 2 min at 92 °C followed by 15 s at 92 °C, 30 s at 50 °C, 8 min at 68 °C for 40 cycles. The relative mitochondrial DNA content was determined by real-time PCR, using COX1 and COX3 primers, normalized to a nuclear-encoded β-actin gene. The following rat primer sequences were used: COX1 (199 bp) forward: 5′-CACAGTAGGGGGCCTAACAG-3′, reverse: 5′-CAAAGTGGGCTTTTGCTCAT-3′; COX3 (244 bp) forward 5′-TCAGGAGTCTCAATTACATG-3′, reverse: 5′-CGTAGTAGACAGACAATTAGG-3′; β-actin (191 bp) forward 5′-GCGGTGACCATAGCCCTCTTT-3′, reverse: 5′-TGCCACTCCCAAAGTAAAGGGTCA-3′. Crossing points were automatically generated by the software and calculation of mitochondrial DNA (mtDNA) damage was made using the Δ2Ct method.

### *2.16. Analysis of citrate synthase activity and glutathione level in NRCM cells*

NRCM cells were seeded at a density of $10^6$ cells/well in 6-well plates and cultured. After the appropriate treatment, cells were harvested, the cell pellet was suspended in ice-cold citrate synthase or GSH cell lysis buffer, then centrifuged for 5 min at 4 °C at 10,000 ×*g*, then the supernatant was collected for further use. Citrate synthase was measured

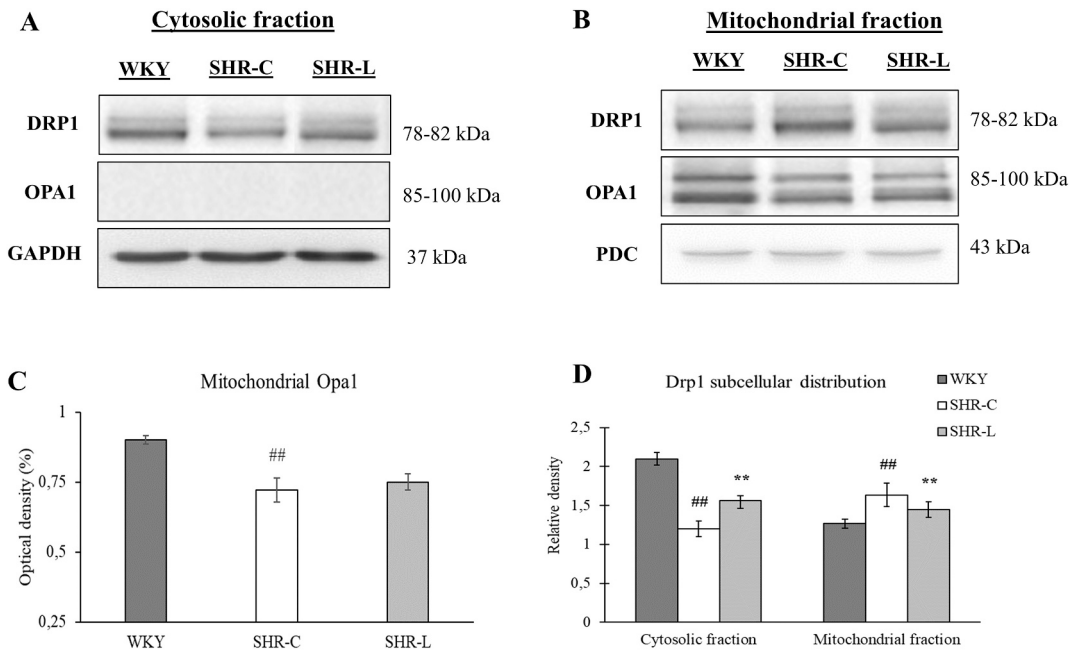


**Fig. 4.** The effect of L-2286 treatment on the intracellular distribution of Drp1 and Opa1 proteins. (A) Representative western blot analysis of Drp1 and Opa1 protein level in the cytosolic fraction. (B) Representative western blot analysis of Drp1 and Opa1 protein amount in the mitochondrial fraction. GAPDH and PDC were used as loading control. (C) The effect of L-2286 treatment on the mitochondrial fusion protein Opa1 in subcellular fractions. (D) The effect of L-2286 treatment on the cellular distribution of Drp1. SHR-C: non-treated spontaneously hypertensive (SHR) rats, SHR-L: SHR rats treated by 5 mg/kg/day L-2286 for 32 weeks. Values are means ± S.E.M., ($n = 4$), $^{\#\#}p < 0.01$ vs WKY, $^{*}p < 0.05$ vs SHR-C, $^{**}p < 0.01$ vs SHR-C.

using a kit from Sigma Aldrich (MAK193) following the manufacturer's instruction. The absorbance was recorded at 412 nm every 5 min for 50 min. The colorimetric product (GSH) was proportional to the enzymatic activity of citrate synthase and normalized to the quantity of cells.

Glutathione was measured using a kit from PromoCell (PK-CA577-K251) following the manufacturer's instructions. The amount of total glutathione was detected using a flourometric plate reader (Ex./Em. = 380 nm/460 nm).

### 2.17. Statistical analysis

All data were expressed as means ± standard error of mean (SEM). First, the homogeneity of the groups was tested by F-test (Levene's test). There were no significant differences among the groups. Comparisons between groups were made using the one-way ANOVA test followed by post hoc correction in SPSS for Windows, version 21.0. The Student's *t*-test was used to compare the mean values of two groups. A value of $p < 0.05$ was considered statistically significant.

## 3. Results

### 3.1. PARP inhibition decreased the left ventricular hypertrophy in spontaneously hypertensive rats

At the beginning of the study the echocardiographic parameters of the three groups did not differ significantly from each other (data not shown). At the age of 42 weeks there was no significant difference in LV systolic function (EF) between the WKY and SHR groups yet. Heart rate did not differ significantly during the anesthesia among the groups. LVESV and LVEDV were increased significantly in SHRs ($p < 0.01$ WKY vs. SHR-C and SHR-L), and these unfavorable alterations were slightly reduced by L-2286 treatment ($p < 0.05$ SHR-L vs SHR-C). The thickness of the septum and posterior wall as well as the left ventricular weight were also increased in SHR groups (indicating the presence of ventricular hypertrophy) comparing to the WKY group ($p < 0.01$), and these parameters could be significantly reduced by the administration of the PARP-inhibitor L-2286 ($p < 0.05$ SHR-L vs. SHR-C group) (Table 1). Moreover, the degree of myocardial hypertrophy was also determined by ventricular weight to body weight ratio (VW/BW, mg/g). This parameter was significantly increased in SHR groups compared to WKY group, but the L-2286 treatment ameliorated this detrimental effect in SHR-L group in comparison to SHR-C group.

Similarly to ejection function in the case of lung wet weight to dry weight ratio (a measure of heart failure), we did not find any significant changes among the groups.

Non-invasive systolic blood pressure measurements of animals were performed to validate hypertension and to demonstrate that L-2286 treatment did not have any significant effects on systolic blood pressure of chronic hypertensive animals (Table 1).

### 3.2. Plasma BNP level in young hypertensive animals

Only slightly elevated plasma BNP levels were found in SHR-C and SHR-L groups (NS vs. WKY group), which means that at this stage of hypertensive heart disease there is no heart failure yet. Of course, the difference between the hypertensive groups was also not significant (Table 1.).

### 3.3. The effect of L-2286 treatment on the activity of PARP enzyme

To detect the effectivity of L-2286 treatment on PARP activity, the auto-PARylation of the PARP-1 enzyme was analyzed in each total western blot sample. The highest degree of poly(ADP-ribosyl)ation was present in the SHR-C group ($p < 0.01$ vs. WKY). L-2286 treatment in the applied dose caused a prominent and significant decrease in the PARP-1 auto-PARylation ($p < 0.01$ SHR-L vs. SHR-C) (Fig. 1).

### 3.4. Effect of PARP inhibition on the structure of interfibrillar mitochondria

Longitudinal sections of myofibrils were evaluated to assess the status of the interfibrillar mitochondria by electron microscopy. In the

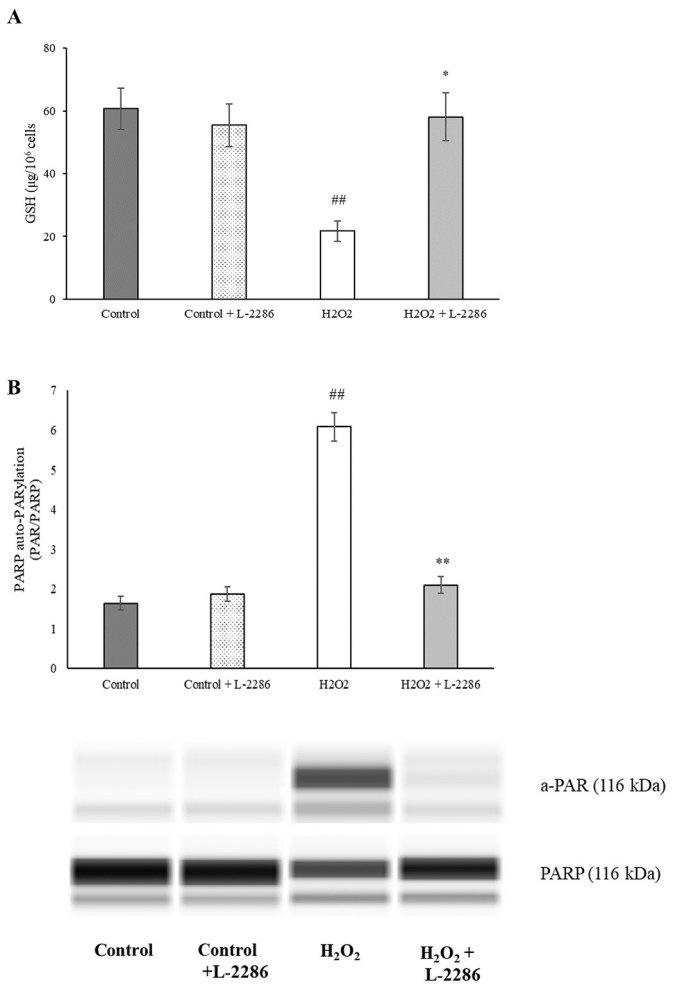


**Fig. 5.** Effect of L-2286 treatment on GSH level and on PARP-1 auto-PARylation in NRCM cells. Comparison of GSH level (μg/$10^6$ cell) among the groups (A). Quantitative analysis of PARP-1 auto-PARylation, representative capillary western immunoassay of PARP and a-PAR expression level is shown (B). Group of cells: Control: cells without any treatment, Control+L-2286: cells incubated with 10 μM L-2286 for 0.5 h, $H_2O_2$: cells stressed with 150 μM $H_2O_2$ for 0.5 h, $H_2O_2$ + L-2286: cells stressed with 150 μM $H_2O_2$ and treated with 10 μM L-2286 for 0.5 h. Values are means ± S.E.M, ($n = 4$). ##$p < 0.01$ vs Control group, *$p < 0.05$ vs $H_2O_2$ group, **$p < 0.01$ vs. $H_2O_2$ group.

WKY group interfibrillar mitochondria are arranged in an orderly manner and their size was quite homogeneous. Ultrastructurally mitochondria are densely filled with regular, wrinkled cristae in normotensive animals (Fig. 2A and D). In untreated SHRs (SHR-C group), mitochondria are morphologically more heterogeneous and a marked decrease in electron density of the mitochondrial matrix was apparent. Mitochondria loosely fills the space among the contractile elements. Altogether, a more disorganized picture was obtained compared to WKY animals. Ultrastructurally, the crista density was decreased, and the dilatation of the intermembrane space could be observed in the SHR-C group (Fig. 2B and E). L-2286 treatment (SHR-L) attenuated these unfavorable alterations, as mitochondria are less fragmented, their matrix was more electrodense and the number of regular cristae and crista junctions was also increased compared to the SHR-C animals (Fig. 2C and F). The myocardium of L-2286 treated SHR rats demonstrated an intermediate phenotype with regional heterogeneity, yet a more preserved inner structure, and cristae numbers of interfibrillar mitochondria ($p < 0.01$ vs SHR-C) (Fig. 2G).

### 3.5. The effect of L-2286 treatment on the size of mitochondria

The whole range of the mitochondrial areas that was found in cardiomyocytes was divided into seven equal ranges of 0.3 $\mu m^2$, in which the relative frequency of mitochondria was determined. Only less than 1% of mitochondria were extremely large (area more than 2.1 $\mu m^2$) in each group of animals. In the WKY group the most common mitochondrial area range was the 0.3–0.6 $\mu m^2$ range (Fig. 3A). In hypertensive control animals (Fig. 3B) about half of the measured mitochondria belonged to the lowest area range (<0.3 $\mu m^2$), however in the WKY group only appr. 20% of mitochondria pertained into this area range. This result indicates a more fragmented phenotype of interfibrillar mitochondria due to hypertension-induced myocardial remodeling and oxidative stress. In L-2286-treated hypertensive animals, however, the distribution of the size of mitochondria was similar to the WKY group, and most mitochondria belonged to the 0.3–0.6 $\mu m^2$ area range (Fig. 3C).

The changes in the mitochondrial size can also be assessed by determining the mean area or the length of mitochondria in each group. Significantly lower values could be seen in the SHR-C group compared to the normotensive group ($p < 0.05$ SHR-C vs. WKY) (Fig. 3D). Regarding both the mean area and longitudinal axis of mitochondria, a significant decrease was apparent in the SHR-C group ($p < 0.01$, SHR-C vs. WKY) compared to the normotensive group (Fig. 3E). The worsening of these parameters were less pronounced in SHR animals treated by L-2286 ($p < 0.01$, SHR-L vs. SHR-C) (Fig. 3C, D, E).

### 3.6. The effect of L-2286 treatment on the subcellular distribution of mitochondrial dynamics-related proteins

Opa1 was not detected in the cytosolic fraction. In mitochondrial fractions of SHR-C samples the Opa1 level was decreased significantly compared to normotensive animals ($p < 0.01$, SHR-C vs. WKY). L-2286 treatment did not influence significantly the decrease of Opa1 level in mitochondria (Fig. 4A-C). Chronic hypertension induced myocardial remodeling did not have any significant effect on overall cellular amount of Drp1 protein in our animal model. Neither did the L-2286 treatment cause any significant alteration in Drp1 protein level (data not shown). To assess the intracellular distribution of Drp1 protein between the cytosolic and mitochondrial compartments, fractionated western blot samples were used. In cytosolic fractions, Drp1 level was the lowest in the non-treated hypertensive control group ($p < 0.01$, SHR-C vs. WKY) (Fig. 4A, D). Inhibition of PARP-1 by L-2286 treatment retained a higher amount of Drp1 in the cytosol ($p < 0.01$ SHR-L vs. SHR-C). On the other hand, the greatest translocation of Drp1 into the mitochondria could be seen in the SHR-C group ($p < 0.01$, SHR-C vs. WKY) (Fig. 4B, D). L-2286 treatment reduced the level of Drp1 in the mitochondrial fraction ($p < 0.05$, SHR-L vs. SHR-C).

### 3.7. The effect of L-2286 treatment on glutathione level and on auto-PARylation in NRCM cells

During oxidative stress there is a decrease in level of GSH, thus GSH/GSSG ratio also decreases. In our experiments $H_2O_2$ induced a significant decrease in GSH level of NRCM cells, indicating oxidative damage. L-2286 treatment on the other hand ameliorated this detrimental effect of oxidative stress (Fig. 5A). To detect the effectivity of L-2286 treatment, the activity of ADP-ribosylation processes were analyzed by capillary western blot in NRCM cell samples. The most pronounced auto-PARylation was seen in $H_2O_2$ group, however the L-2286 treatment alleviated this unfavorable effect (Fig. 5B).

### 3.8. Morphological changes in the mitochondrial network

In control NRCM cells the mitochondrial reticulum was normal with long, regular shape (Fig. 6A). However, oxidative stress induced marked

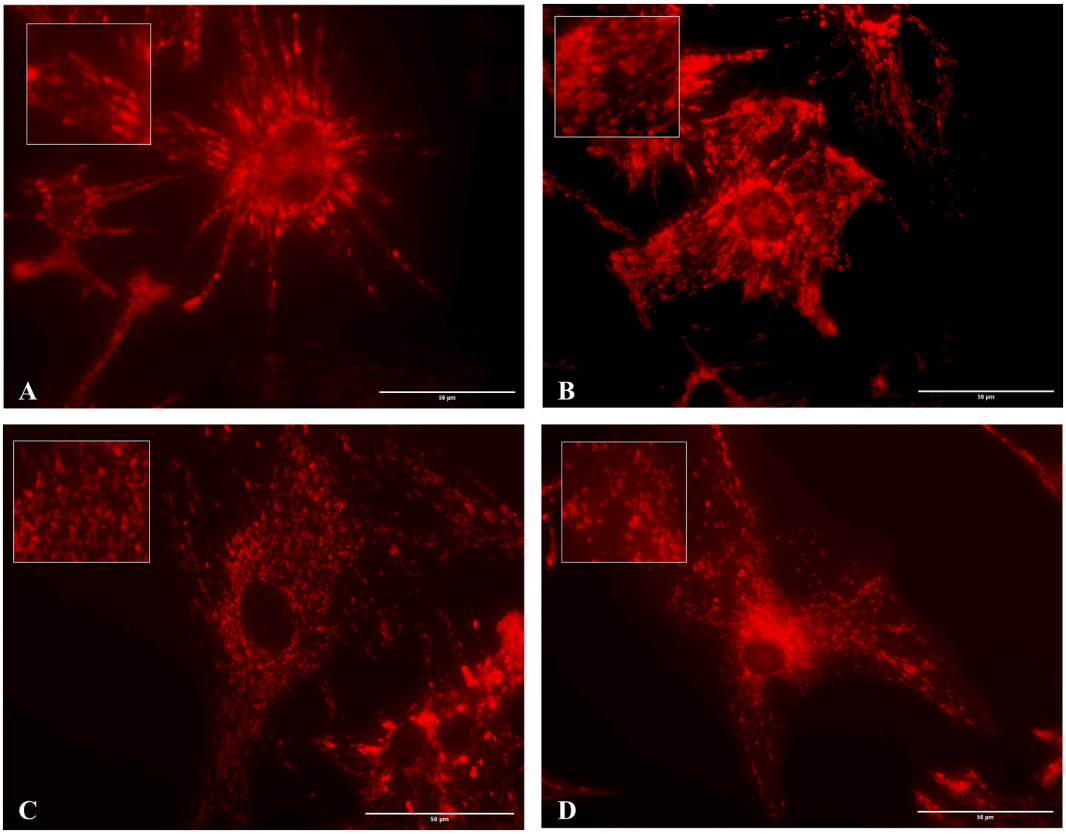


**Fig. 6.** L-2286 treatment protects against oxidative stress-induced mitochondrial fragmentation in neonatal rat cardiomyocytes. The inserts show the filamentous and fragmented states, showing that L-2286 protected the mitochondrial network. Groups: A: Control, B: Control + L-2286, C: $H_2O_2$, D: $H_2O_2$ + L-2286; Mitochondria were labelled by 300 nM MitoTracker Red CMXRos.

morphological changes, the mitochondrial network became fragmented, and consequently small, dot-like mitochondria could be observed (Fig. 6C). L-2286 treatment protected the mitochondrial network against oxidative stress induced damage in NRCMs, and therefore the mitochondrial network remained reticular, similarly to the control cells (Fig. 6D).

### *3.9. Effect of L-2286 on cellular levels and subcellular distribution of fission-fusion regulator proteins*

Our data showed that L-2286 treatment causes significant increase in the amount of the mitochondrial fusion proteins Mfn2 and Opa1 compared to the stressed group, and also compared to the control group ($p < 0.01$ $H_2O_2$ + L-2286 vs. $H_2O_2$ and vs. Control) (Fig. 7A and B), but no significant change was observed in the expression level of Mfn1 protein (Fig. 7C).

Due to L-2286 treatment, the level of mitochondrial fission proteins, Drp1 ($p < 0.05$) and Fis1 ($p < 0.01$) showed a marked decrease as compared to the stressed group (Fig. 8A and B), where these values were the highest ($p < 0.01$ $H_2O_2$ vs. Control). We examined the phosphorylation state of Drp1 protein too, because the phosphorylation of Drp1 at Serine 616 residues promotes mitochondrial fission, however, the phosphorylation of the Drp1 Serine 637 residue inhibits the enzyme activity and its translocation into the mitochondria. We have proved that L-2286 treatment causes significant decrease in the phosphorylation state of Drp1 at Serine 616 residues ($p < 0.01$, $H_2O_2$ + L-2286 vs. $H_2O_2$ group), moreover PARP-inhibition causes considerable increase in phosphorylation state of Drp1 at Serine 637 residue compared to stressed group ($p < 0.01$, $H_2O_2$ + L-2286 vs. $H_2O_2$) (Fig. 8C and D).

We also aimed to determine the subcellular distribution of Drp1 and Opa1 proteins between the cytosolic and mitochondrial compartments of NRCMs, to gain insight into the molecular background of attenuated fission processes and preserved inner mitochondrial membrane structure. Opa1 is not detectable in the cytosol (Fig. 9B). However, in the mitochondrial fraction of L-2286 treated stressed cells the level of Opa1 increased significantly (Fig. 9A) compared to stressed only group ($p < 0.01$, $H_2O_2$ + L-2286 vs. $H_2O_2$). The amount of cytosolic Drp1 in the stressed only group ($H_2O_2$) was the lowest. Inhibition of PARP-1 by L-2286 treatment retained a significantly higher amount of Drp1 in the cytosol ($p < 0.01$ $H_2O_2$ + L-2286 vs. $H_2O_2$). Therefore, it could be stated that the intracellular Drp1 localization was greatly influenced by PARP-inhibition, because the level of Drp1 protein was significantly lower in the mitochondrial fraction and higher in the cytosolic fraction of treated cells (Fig. 9B) compared to stressed only NRCM cells ($p < 0.01$, $H_2O_2$ + L-2286 vs. $H_2O_2$).

### *3.10. Examination of mitochondrial function via membrane potential and oxygen consumption rate*

We examined the effect of PARP-inhibition on mitochondrial membrane potential using JC-1, a cell-permeable voltage-sensitive fluorescent mitochondrial dye (Fig. 10). JC-1 emits red fluorescence if the mitochondrial membrane potential is high (aggregated dye), while depolarized mitochondria emit green fluorescence (monomer dye). Fluorescent microscopy showed strong red and weak green fluorescence in the control group, which indicates normal, healthy mitochondrial membrane potential (high $\Delta\Psi m$). Mitochondrial membrane depolarized due to $H_2O_2$ stress, resulting in weaker red and stronger green fluorescence. The addition of L-2286 to hydrogen peroxide stressed cells, the decrease in the mitochondrial membrane potential was found to be smaller, therefore red and green fluorescence values were similar to that of control cells (Fig. 10A). Quantifying these changes (Fig. 10B) we

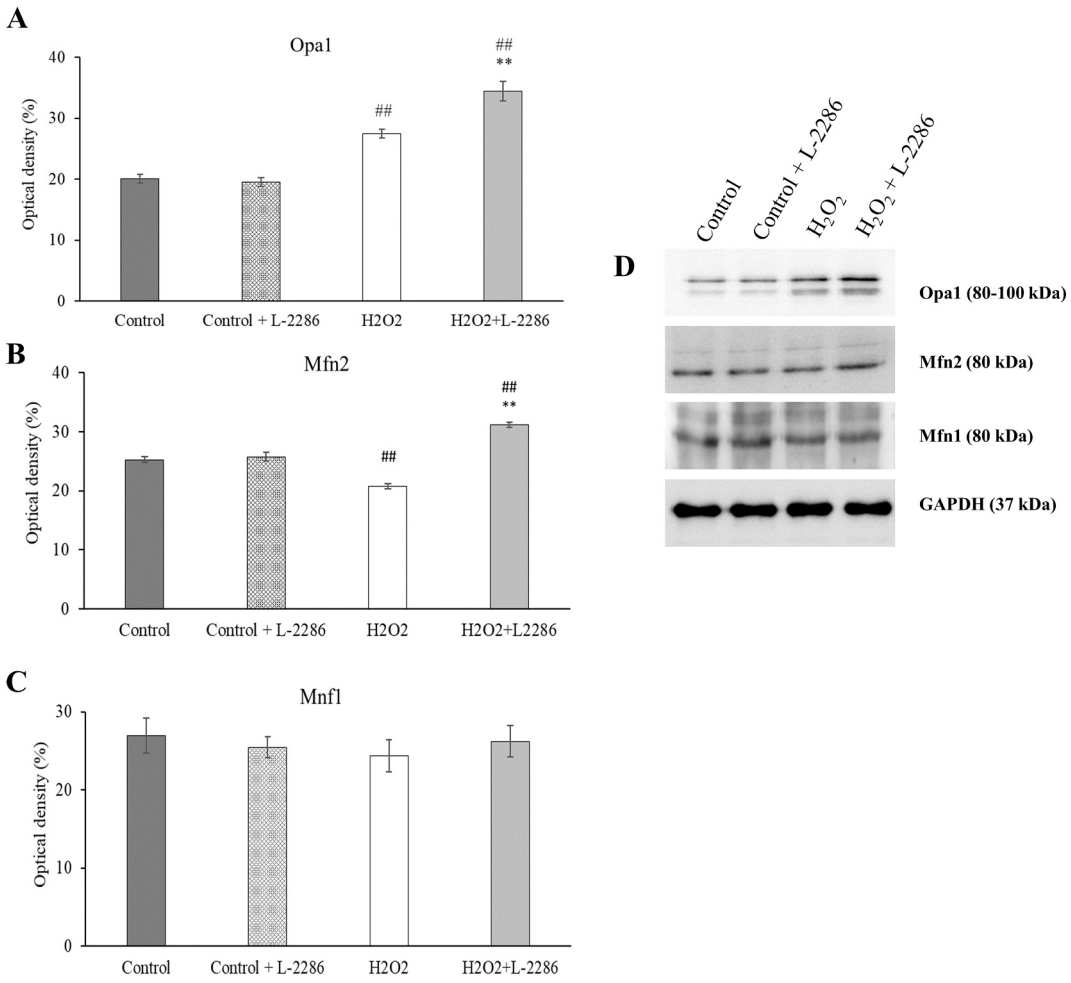


**Fig. 7.** Effect of L-2286 treatment on the level of mitochondrial fusion regulator proteins in NRCM cells. Quantitative analysis of mitochondrial fusion related (A) Opa1, (B) Mfn2 and (C) Mfn1 protein levels. (D) Representative western blot analysis of Opa1 and Mfn2 proteins in NRCM cells. GAPDH was used as loading control. Group of cells: Control: cells without any treatment, Control+L-2286: cells incubated with 10 μM L-2286 for 0.5 h, $H_2O_2$: cells stressed with 150 μM $H_2O_2$ for 0.5 h, $H_2O_2$ + L-2286: cells stressed with 150 μM $H_2O_2$ and treated with 10 μM L-2286 for 0.5 h. Values are means ± S.E.M, ($n = 4$). ##$p < 0.01$ vs Control group, **p < 0.01 vs. $H_2O_2$ group.

could observe that the mitochondrial membrane potential is reduced due to oxidative stress ($p < 0.05$, $H_2O_2$ vs. Control), and this unfavorable change was moderated by L-2286 treatment in our cell culture model (p < 0.05, $H_2O_2$ + L-2286 vs. $H_2O_2$).

To determine the mitochondrial energy metabolism and respiratory function, we used the Agilent Seahorse XFp Analyzer system and the Agilent Seahorse XFp Cell Mito Stress Test (Fig. 11A and B). L-2286 itself had no effect on the rate of mitochondrial respiration. However, we observed that (Fig. 11A) $H_2O_2$ treatment decreased the basal respiration, the maximal respiration, the spare respiratory capacity and the ATP production as a result of $H_2O_2$-induced oxidative damage compared to the Control group ($p < 0.01$, $H_2O_2$ vs. Control). Due to L-2286 treatment the spare respiratory capacity, which is a measure of the ability of cells to respond to increased energy demand or under stress, and the ATP production ability was increased in a significant manner ($p < 0.05$, $H_2O_2$ + L-2286 vs. $H_2O_2$).

### 3.11. *The effect of L-2286 treatment on mitochondrial biogenesis*

In our study we examined the expression and activation levels of proteins involved in mitochondrial biogenesis. In non-stressed cells there was no difference between groups. L-2286 treatment on the other hand causes a significant increase in the expression level of the major regulator protein PGC1α in stressed NRCMs ($p < 0.01$, $H_2O_2$ + L-2286 vs. $H_2O_2$) (Fig. 12A). The activity of CREB was also evaluated measuring its phosphorylation level. CREB is involved in the PGC-1α activation. Our data showed that L-2286 treatment causes a considerable increase in the phosphorylation of CREB at serine 133 compared to the stressed group ($p < 0.01$, $H_2O_2$ + L-2286 vs. $H_2O_2$) (Fig. 12B). The mitochondrial content of NRCM cells was evaluated by estimating the protein content of the mitochondrial voltage-dependent anion channel protein (VDAC), which is ubiquitously expressed and located in the outer mitochondrial membrane. Our data showed that hydrogen peroxide caused a significant decrease in the amount of VDAC compared to non-stressed cells (p < 0.05, $H_2O_2$ vs. Control). L-2286 treatment prevented this decrease, moreover the highest VDAC amount could be seen in the $H_2O_2$ + L-2286 group (p < 0.01, $H_2O_2$ + L-2286 vs. $H_2O_2$ and vs. Control) (Fig. 12C).

To support more preciously the effect of PARP-inhibition on mitochondrial biogenesis and enhanced cellular amount of mitochondria, further investigations were made. The electron transfer chain complexes located on the inner mitochondrial membrane are essential for mitochondrial function. We measured the level of NDUFs1 and UQCRC1 proteins, which are subunits of the respiratory chain proteins NADH-ubiquinone oxidoreductase and Ubiquinol Cytochrome c Reductase (Fig.12D and E). Our results showed that hydrogen-peroxide caused a significant decrease in the amount of NDUFs1 and UQCRC1 proteins compared to non-stressed cells ($p < 0.01$, $H_2O_2$ vs Control). In addition, hydrogen-peroxide stress with L-2286 treatment prevented this

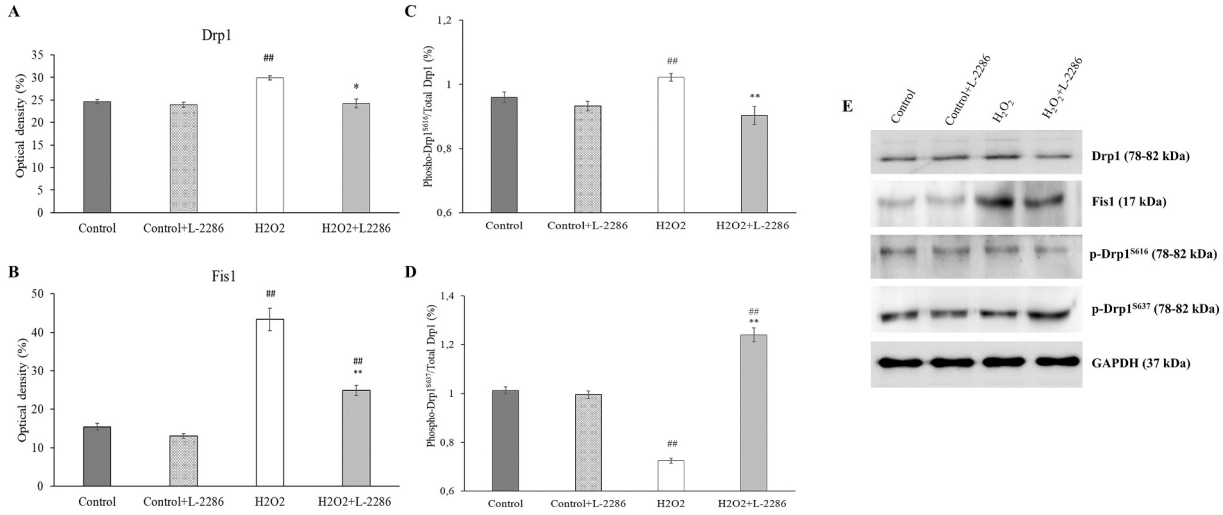


**Fig. 8.** Effect of L-2286 treatment on mitochondrial fission mediators in NRCM cells. (A) Quantitative analysis of the amount of Drp1 protein, (B) Quantitative analysis of the Fis1 protein expression level, (C) Quantitative analysis of the phosphorylation of Drp1 S616 residues, (D) Quantitative analysis of the phosphorylation of Drp1 S637 residues. (E) Representative Western-blot pictures of Fis1, Drp1 levels as well as phosphorylation of phospho-Drp1$^{S616}$ and phospho-Drp1$^{S637}$ residues. GAPDH was used as loading control. Group of cells: Control: cells without any treatment, Control+L-2286: cells incubated with 10 μM L-2286 for 0.5 h, $H_2O_2$: cells stressed with 150 μM $H_2O_2$ for 0.5 h, $H_2O_2$ + L-2286: cells stressed with 150 μM $H_2O_2$ and treated with 10 μM L-2286 for 0.5 h. Values are means ± S.E.M, ($n = 4$). $^{\#\#}p < 0.01$ vs. Control group, $^{**}p < 0.01$ vs. $H_2O_2$ group, $^{*}p < 0.05$ vs $H_2O_2$ group.

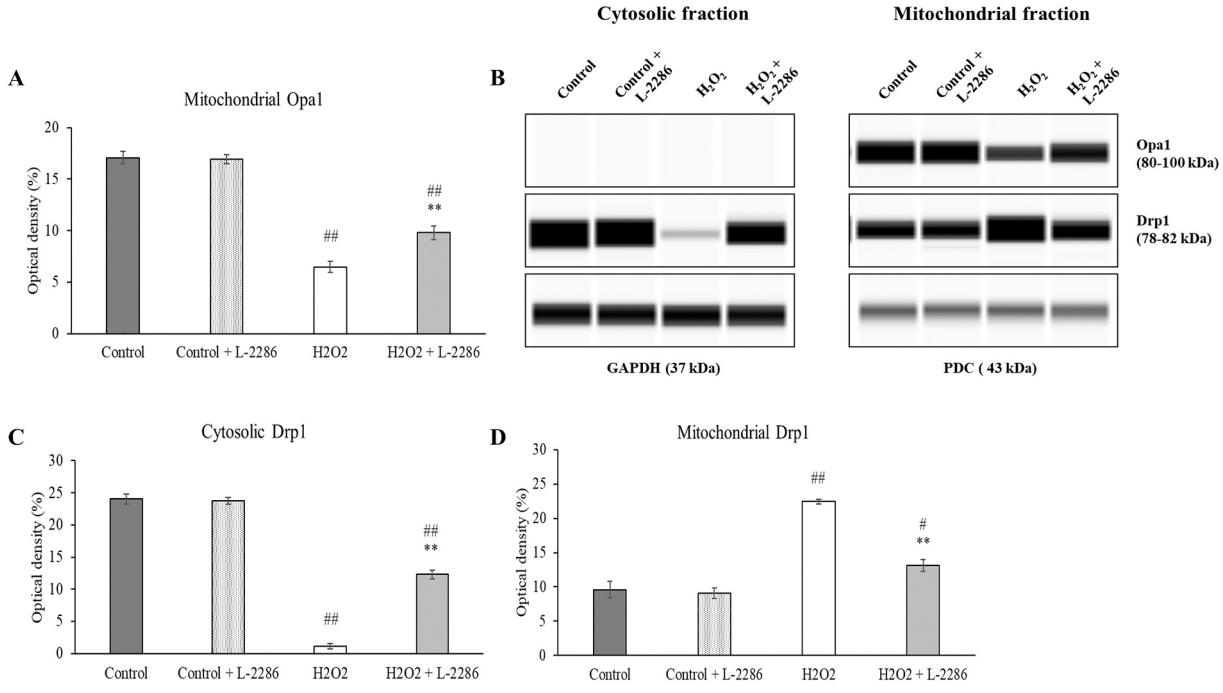


**Fig. 9.** Effect of L-2286 on the intracellular distribution of Drp1 and Opa1 proteins. (A) Quantitative analysis of Opa1 level in mitochondrial fraction. (B) Representative capillary western immunoassay of Opa1 and Drp1 expression level is shown. GAPDH was used for cytosolic, PDC was used for mitochondrial fraction as loading control, (C) Quantitative analysis of the Drp1 protein level in cytosolic fraction. (D) Quantitative analysis of mitochondrial Drp1. Group of cells: Control: cells without any treatment, Control+L-2286: cells incubated with 10 μM L-2286 for 0.5 h, $H_2O_2$: cells stressed with 150 μM $H_2O_2$ for 0.5 h, $H_2O_2$ + L-2286: cells stressed with 150 μM $H_2O_2$ and treated with 10 μM L-2286 for 0.5 h. Values are means ± S.E.M, (n = 4), $^{\#\#}p < 0.01$ vs. Control group, $^{\#}p < 0.05$ vs. Control group, $^{**}p < 0.01$ vs. $H_2O_2$ group.

decrease, moreover the highest NDUFs1 and UQCRC1 level could be seen in this group ($p < 0.01$, $H_2O_2$ + L-2286 vs. $H_2O_2$).

The relative mitochondrial DNA content was determined by "real-time" PCR, using COX1 and COX3 primers, normalized to a nuclear-encoded β-actin gene. We found that L-2286 treatment increased the relative expression level of both tested genes (Fig. 12G and H). Moreover, we investigated the citrate synthase activity in NRCM cells. Citrate synthase (CS) activity was reduced in hydrogen-peroxide stressed group approximately 55% compared to control group. In the L-2286 treated group, the citrate synthase activity was increased almost 20% in comparison to stressed group (Fig. 12I).

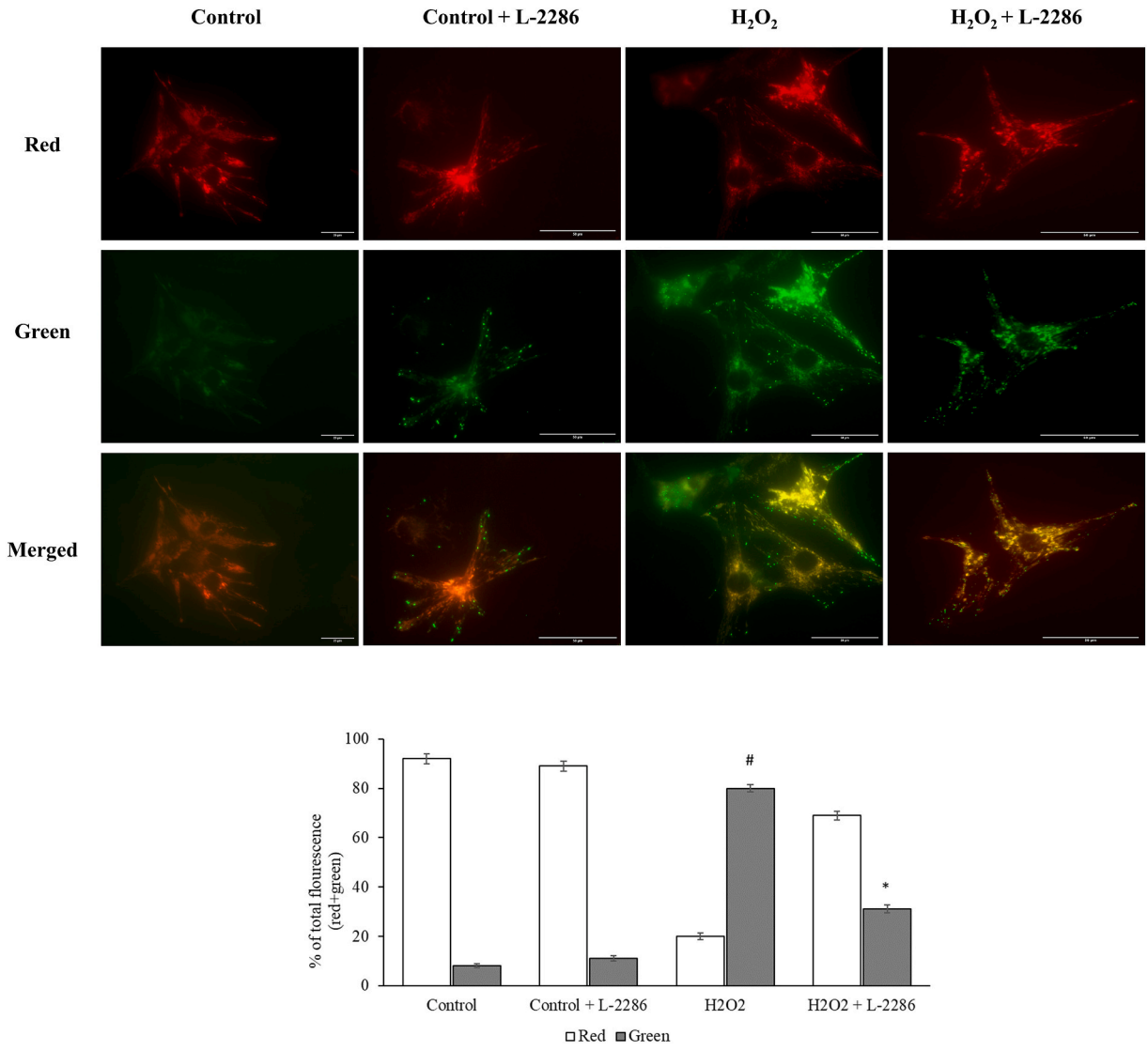


**Fig. 10.** The L-2286 treatment prevents mitochondrial membrane depolarization in hydrogen peroxide-stressed NRCM cells. Representative images of three independent experiments are presented. (B) Quantitative analysis of oxidative stress-induced mitochondrial membrane depolarization and its reduction by L-2286 treatment in NRCM cells. Group of cells: Control: cells without any treatment, Control+L-2286: cells incubated with 10 μM L-2286 for 0.5 h, $H_2O_2$: cells stressed with 150 μM $H_2O_2$ for 0.5 h, $H_2O_2$ + L-2286: cells stressed with 150 μM $H_2O_2$ and treated with 10 μM L-2286 for 0.5 h. Values are mean ± S.E.M. $^{\#}p < 0.05$ vs. Control group, $^{*}p < 0.05$ vs. $H_2O_2$ group.

### 3.12. The effect of L-2286 treatment on mitochondrial genome integrity

In the present study we used $H_2O_2$ exposure as a toxic agent having DNA damaging potential. Using the real-time detection of long-range PCR (14,958 bp; LRPCR) and short-range (210 bp; SRPCR) we examined the impact of 150 μM $H_2O_2$ on mtDNA integrity. These data show that oxidative stress induced a significant damage of the mtDNA in the stressed group ($p < 0.01$ vs. Control group). In the treated group the mitochondrial DNA was less fragmented, its relative expression level showed a marked, almost 4-fold increase compared to the stressed group ($p < 0.01$, $H_2O_2$ + L-2286 vs. $H_2O_2$) (Fig. 13).

## 4. Discussion

The major finding of this study is that pharmacological PARP-inhibition protects against the development of hypertensive heart disease via the maintenance of physiological mitochondrial structure and function.

SHR model was used in our experiments as a relevant animal model of essential hypertension in humans [29,30]. Marked hypertensive heart failure developed in hypertensive animals by the end of the study (42 weeks), although without manifesting any signs of heart failure. These are in accordance with previous works in the literature [21,23,31]. In non-treated SHR animals the left ventricular wall thicknesses and calculated LV mass increased markedly compared to normotensive WKY rats. The volumes of left ventricle also increased, however, the systolic left ventricular function remained normal. In line with the unchanged EF, the heart failure biomarker BNP level was also practically unchanged (Table 1) [32]. PARP-inhibition caused a significant decrease in parameters indicating cardiac hypertrophy, what is also in accord with previous results [13,21,23].

Nowadays there is a substantial literature regarding the cytoprotective effects of PARP inhibition among various pathological conditions [33–35]. PARP-inhibitors beside their "orthodox" $NAD^+$-preserving effect, can also influence several signal transduction pathways. It was proved, that they activate the prosurvival signaling (PI3K/Akt-1/GSK-3β, PKCε), which in turn protects mitochondria and therefore the cell survival during oxidative stress [23,36]. In addition, PARP-inhibition

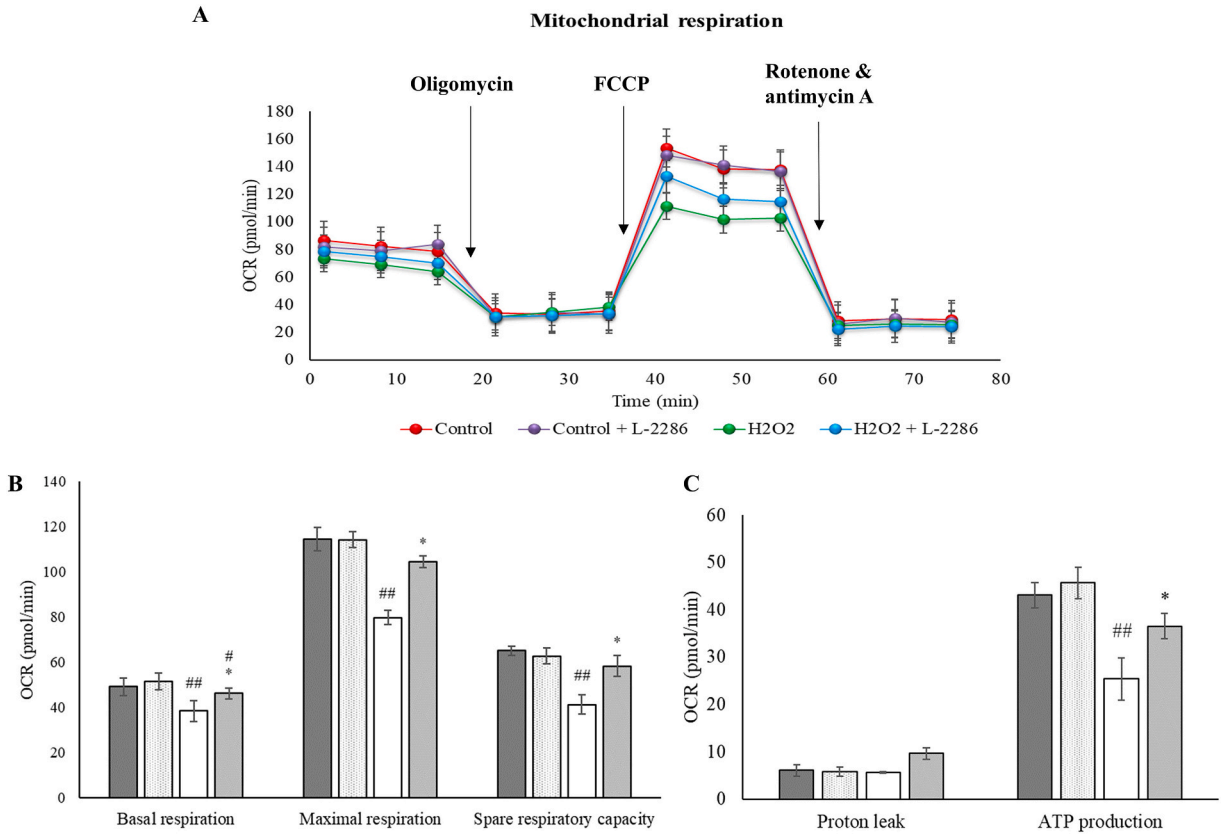


**Fig. 11.** The effect of L-2286 treatment on the oxygen consumption rate in NRCM cells. (A) oxygen consumption rate (OCR) in NRCM cells, measured by Seahorse XFp Analyzer. (B) Basal respiration, maximal respiration and spare respiratory capacity in NRCM cells. (C) Proton leak and ATP production ability in NRCM cells. Group of cells: Control: cells without any treatment, Control+L-2286: cells incubated with 10 μM L-2286 for 0.5 h, $H_2O_2$: cells stressed with 150 μM $H_2O_2$ for 0.5 h, $H_2O_2$ + L-2286: cells stressed with 150 μM $H_2O_2$ and treated with 10 μM L-2286 for 0.5 h. Values are mean ± S.E.M, ($n = 4$). $^{\#\#}p < 0.01$ vs. Control group, $^{\#}p < 0.05$ vs. Control group, $^{*}p < 0.05$ vs. $H_2O_2$ group.

suppresses the activity of MAP kinases (JNK, p38 MAPK) through the enhanced MKP-1 production. MKP-1 downregulation, however, leads to increased JNK phosphorylation, and to the activation of mitochondrial fission and mitophagy and therefore to compromised mitochondrial energy production [23,37,38].

Moreover, the direct mitochondrial protective effect of PARP-inhibition was already confirmed by our workgroup in isolated mitochondria earlier [39].

This knowledge led us in our recent work to focus on the effects of PARP-inhibition on various mitochondrial processes as well as on structural and functional alterations of mitochondria during oxidative stress situations. The effectivity of the applied PARP-inhibitor (L-2286) was checked by measuring the auto-PARylation of the PARP enzyme (Fig. 1.).

The interfibrillar mitochondria (IFM) having a profound role in supplying the energy demand of cardiac work physiologically tightly fills the space between the contractile elements of cardiomyocytes. In the myocardium of 42-week-old untreated SHRs (SHR-C), mitochondria became morphologically more heterogeneous, they were loosely arranged between the myofilaments, the dilation of cristae spaces was apparent, and the size of mitochondria was also decreased (Fig. 2). These alterations indicate a more fragmented phenotype of IFM due to chronic hypertension induced oxidative stress (Fig. 3). In contrast, in the myocardium of L-2286 treated SHRs (SHR-L) mitochondria were less fragmented, and they showed higher cristae density.

The fragmentation of mitochondria is regulated by the balance of fusion-fission processes. To monitor these processes, the amount and subcellular distribution of the main fusion promoter Opa1 and the fission-inducing factor Drp1 was determined (Fig. 4). In our animal model chronic hypertension did not have any significant effects on the cellular level of proteins playing a part in the fission and fusion. However, the subcellular distribution of Drp1 was altered, its translocation to the mitochondrial fraction increased, which is a starting point of provoking fragmentation of mitochondria. Drp1 translocation and therefore the fission of mitochondria was blocked by the L-2286.

To study the effect of PARP-inhibition on mitochondrial structure and function in a more detailed manner, in vitro experiments were carried out using hydrogen peroxide-induced severe oxidative stress in neonatal rat cardiomyocytes (NRCM).

Oxidative stress was quantified in NRCM cells measuring the glutathione level and the activity of PARylation processes. The decreased GSH level and increased auto-PARylation of PARP-1 enzyme showed that in hydrogen peroxide-stressed cells a significant oxidative stress is present. Both unfavorable changes could be diminished by pharmacological PARP-inhibition using L-2286. (Fig. 5). Mitochondria form a dynamic network in the cell, which is determined by the balance of fusion-fission processes. During oxidative stress, the mitochondrial network becomes fragmented, which has a central role in the cellular survival. Imbalanced mitochondrial dynamics are associated with a range of diseases that are broadly characterized by impaired mitochondrial function and increased cell death [40]. L-2286 treatment prevented the oxidative stress-induced mitochondrial fragmentation in NRCM cells (Fig. 6). In the background of this phenomenon, increased amount of fusion proteins (Opa1, Mfn2) could be seen in stressed NRCMs receiving PARP-inhibitor (Fig. 7). However, the expression level of fission mediators (Fis1, Drp1) were decreased by L-2286 treatment (Fig. 8). The activation and mitochondrial translocation of Drp1 is regulated by the phosphorylation of Drp1. Phosphorylation of Drp1 at

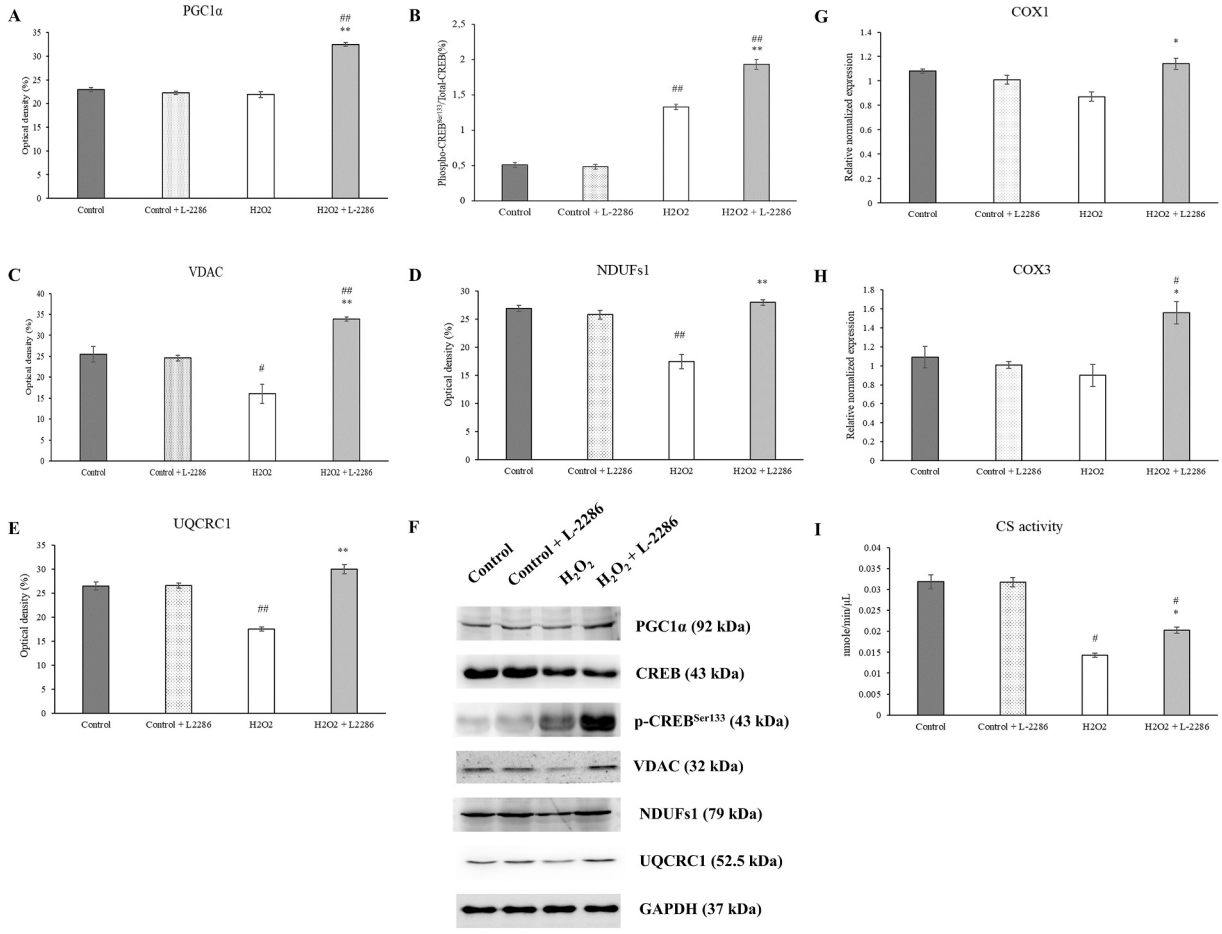


**Fig. 12.** Effect of L-2286 treatment on the amount of mitochondrial biogenesis related proteins, relative DNA content and citrate synthase activity. (A) Quantitative analysis of the amount of PGC-1α and VDAC (A, C). Quantitative analysis of phosphorylation state of CREB protein (B). Quantitative analysis of the electron transport chain complex I and III proteins, NDUFs1 (D) and UQCRC1 (E). Representative Western blot images of PGC1α, CREB, VDAC, NDUFs1 and UQCRC1 expression level, as well as phospho-Creb$^{Ser133}$ are shown (F). GAPDH was used for a loading control. Relative expression level of electron transport chain complex IV genes (COX1 and COX3) are presented (G, H). Comparison of citrate synthase activity in NRCM cells (I). Group of cells: Control: cells without any treatment, Control+L-2286: cells incubated with 10 μM L-2286 for 0.5 h, $H_2O_2$: cells stressed with 150 μM $H_2O_2$ for 0.5 h, $H_2O_2$ + L-2286: cells stressed with 150 μM $H_2O_2$ and treated with 10 μM L-2286 for 0.5 h. Values are mean ± S.E.M, (n = 4). $^{\#\#}p < 0.01$ vs. Control group, $^{\#}p < 0.05$ vs Control group, $^{**}p < 0.01$ vs. $H_2O_2$ group.

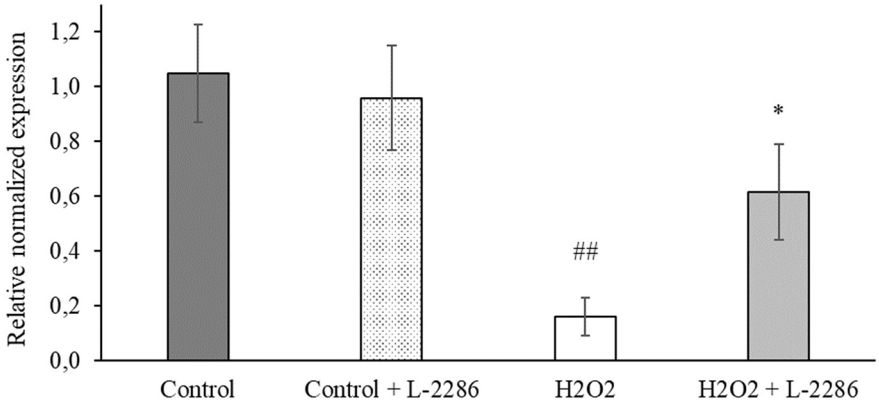


**Fig. 13.** Effect of L-2286 treatment on oxidative stress-induced mitochondrial DNA damage. After the appropriate treatment, the total DNA was isolated for LRPCR and SRPCR analysis as indicated in Methods. mtDNA damage was calculated using the Δ2Ct method. Control group: cells without any treatment, L-2286 group: cells with only 10 μM L-2286 for 0.5 h, $H_2O_2$ group: cells with 150 μM $H_2O_2$ for 0.5 h, $H_2O_2$ + L-2286 group: cells with 150 μM $H_2O_2$ and 10 μM L-2286 for 0.5 h. Values are mean ± SEM, (n = 4), $^{\#\#}p < 0.01$ vs. Control group, $^{*}p < 0.05$ vs. $H_2O_2$ group.

Serine 616 promotes mitochondrial fission, but Drp1 Serine 637 phosphorylation inhibits the activity and translocation of Drp1 to the mitochondria [41,42]. L-2286 treatment caused significant decrease in the phosphorylation of Drp1 at Serine 616, while an increase in the Drp1 phosphorylation at Serine 637 (Fig. 8). In accordance with this result, PARP-inhibition retained Drp1 in the cytosolic fraction despite oxidative stress, while the level of Drp1 in the mitochondrial fraction was significantly lower than in non-treated stressed cardiomyocytes (Fig. 9). These results suggest that L-2286 treatment can reduce mitochondrial fission as the translocation and anchorage of Drp1 to the outer mitochondrial membrane is diminished. Due to PARP-1 inhibition, the mitochondrial Opa1 content regulating the integrity and fusion of inner mitochondrial

membranes was increased (Fig. 9).

The maintenance of physiological mitochondrial structure through shifting mitochondrial dynamics toward the fusion, yields in a normal mitochondrial membrane potential despite oxidative stress [43,44]. Therefore, the above-mentioned favorable effects of L-2286 treatment on mitochondrial structure and fission-fusion processes result in preserving physiological mitochondrial membrane potential that is essential in the normal mitochondrial function (Fig. 10). Thus L-2286 treatment reverted the oxidative stress-induced decrease in mitochondrial function that was determined by a Seahorse XFp Analyzer. PARP-inhibition improved the spare respiratory capacity, which is a measure of the ability of the cell to respond to increased energy demand or under stress, and the ATP production ability in NRCM cells despite the presence of oxidative stress (Fig. 11).

Mitochondrial respiratory chain complexes are encoded on mtDNA, which is particularly sensitive to oxidative stress [35,45]. Our results suggested that hydrogen-peroxide caused mtDNA breaks, which hinders the transcription of genes coding the proteins of electron transport chain (ETC) [46]. In L-2286 treated NRCMs significantly less DNA breaks were observed, therefore it can be stated that PARP-inhibition can maintain the integrity of mitochondrial genome, therefore it can maintain the normal production of mitochondrial ETC complexes in stressed cells (Fig. 13).

The mitochondrial biogenesis can also be an important factor of energy production in cells [47]. It was found that mitochondrial content characterized by the amount of VDAC protein and by the citrate synthase activity was decreased due to oxidative stress and this could be reverted by L-2286 treatment (Fig. 12). The relative DNA content of ETC complex IV as well as the expression level of ETC I and III proteins were also significantly increased due to PARP-inhibitor treatment showing an enhanced cellular mitochondrial content in L-2286-treated cells. Mitochondrial biogenesis is regulated among others by the activation of PGC-1α via CREB activation. In oxidative stress situations L-2286 treatment induces activation of Akt protein, which promotes cell survival. A growing body of recent evidence has suggested that the activated Akt provides an activating phosphorylation (Ser133) to the CREB protein. The PGC1α gene promoter region exhibits a well-conserved binding site for CREB, which drives PGC1α expression after its activation [48–50]. In stressed NRMC cells L-2286 caused a marked elevation in the amount and activity of both regulator proteins.

We have found that PARP-inhibitor treatment exerted wide-range positive effects on mitochondria during stress situations. PARP-inhibition shifted the mitochondrial dynamics toward fusion, increased biogenesis yielding in higher cellular mitochondrial content. Moreover, the ultrastructure and function of mitochondria were also preserved. All these effects can be at least partly in the background of its antioxidant, cyto- and cardioprotective effect.

## 5. Conclusion

In conclusion, pharmacological PARP-inhibition prevents cardiomyocytes against both chronic low-intensity oxidative stress as well as against acute, extensive oxidative damage by its mitochondrial protective effect. Modulation of mitochondrial dynamics and biogenesis can be a promising therapeutical target in the prevention and treatment of hypertension-induced myocardial remodeling and heart failure.

## Author agreement

The authors have approved of and have agreed to submit the manuscript to this journal.

## Declaration of competing interest

The authors declare that they have no known competing financial interests or personal relationships that could have appeared to influence the work reported in this paper.

## Acknowledgements

This study was supported by the Hungarian National Research Foundations Grant (GINOP-2.3.2-15-2016-00048) and the Higher Education Institutional Excellence Programme of the Ministry for Innovation and Technology in Hungary, within the framework of the 1st thematic programme of the University of Pécs (2020-4.1.1-TKP2020).

## References

[1] K.T. Mills, J.D. Bundy, T.N. Kelly, J.E. Reed, P.M. Kearney, K. Reynolds, J. Chen, J. He, Global disparities of hypertension prevalence and control: a systematic analysis of population-based studies from 90 countries, Circulation 134 (2016) 441–450, https://doi.org/10.1161/CIRCULATIONAHA.115.018912.

[2] F.H. Messerli, S.F. Rimoldi, S. Bangalore, The transition from hypertension to heart failure: contemporary update, JACC Heart Fail 5 (2017) 543–551, https://doi.org/10.1016/j.jchf.2017.04.012.

[3] Arantxa González, Susana Ravassa, Begoña López, María U. Moreno, Javier Beaumont, Gorka San José, Ramón Querejeta, Antoni Bayés-Genís, Javier Díez, Myocardial remodeling in hypertension, Hypertension 72 (2018) 549–558, https://doi.org/10.1161/HYPERTENSIONAHA.118.11125.

[4] P. Pellicori, M.J.I. Khan, F.J. Graham, J.G.F. Cleland, New perspectives and future directions in the treatment of heart failure, Heart Fail. Rev. 25 (2020) 147–159, https://doi.org/10.1007/s10741-019-09829-7.

[5] A. van der Pol, W.H. van Gilst, A.A. Voors, P. van der Meer, Treating oxidative stress in heart failure: past, present and future, Eur. J. Heart Fail. 21 (2019) 425–435, https://doi.org/10.1002/ejhf.1320.

[6] D.J. Grieve, A.M. Shah, Oxidative stress in heart failureMore than just damage, Eur. Heart J. 24 (2003) 2161–2163, https://doi.org/10.1016/j.ehj.2003.10.015.

[7] S.-B. Ong, Å.B. Gustafsson, New roles for mitochondria in cell death in the reperfused myocardium, Cardiovasc. Res. 94 (2012) 190–196, https://doi.org/10.1093/cvr/cvr312.

[8] J. González, N. Valls, R. Brito, R. Rodrigo, Essential hypertension and oxidative stress: new insights, World J. Cardiol. 6 (2014) 353–366, https://doi.org/10.4330/wjc.v6.i6.353.

[9] M. Dizdaroglu, P. Jaruga, Mechanisms of free radical-induced damage to DNA, Free Radic. Res. 46 (2012) 382–419, https://doi.org/10.3109/10715762.2011.653969.

[10] L.A. Pham-Huy, H. He, C. Pham-Huy, Free radicals, antioxidants in disease and health, Int. J. Biomed. Sci. IJBS 4 (2008) 89–96.

[11] E.E. Alemasova, O.I. Lavrik, Poly(ADP-ribosyl)ation by PARP1: reaction mechanism and regulatory proteins, Nucleic Acids Res. 47 (2019) 3811–3827, https://doi.org/10.1093/nar/gkz120.

[12] X. Luo, W.L. Kraus, On PAR with PARP: cellular stress signaling through poly(ADP-ribose) and PARP-1, Genes Dev. 26 (2012) 417–432, https://doi.org/10.1101/gad.183509.111.

[13] P. Pacher, C. Szabó, Role of poly(ADP-ribose) polymerase 1 (PARP-1) in cardiovascular diseases: the therapeutic potential of PARP inhibitors, Cardiovasc. Drug Rev. 25 (2007) 235–260, https://doi.org/10.1111/j.1527-3466.2007.00018.x.

[14] L. Virág, A. Robaszkiewicz, J.M. Rodriguez-Vargas, F.J. Oliver, Poly(ADP-ribose) signaling in cell death, Mol. Asp. Med. 34 (2013) 1153–1167, https://doi.org/10.1016/j.mam.2013.01.007.

[15] M. Kindo, S. Gerelli, J. Bouitbir, A.-L. Charles, J. Zoll, T. Hoang Minh, L. Monassier, F. Favret, F. Piquard, B. Geny, Pressure overload-induced mild cardiac hypertrophy reduces left ventricular transmural differences in mitochondrial respiratory chain activity and increases oxidative stress, Front. Physiol. 3 (2012), https://doi.org/10.3389/fphys.2012.00332.

[16] C. Richter-Landsberg, U. Vollgraf, Mode of cell injury and death after hydrogen peroxide exposure in cultured oligodendroglia cells, Exp. Cell Res. 244 (1998) 218–229, https://doi.org/10.1006/excr.1998.4188.

[17] J.J.P. Gille, H. Joenje, Cell culture models for oxidative stress: superoxide and hydrogen peroxide versus normobaric hyperoxia, Mutat. Res. 275 (1992) 405–414, https://doi.org/10.1016/0921-8734(92)90043-O.

[18] A. Pálfi, A. Tóth, G. Kulcsár, K. Hantó, P. Deres, E. Bartha, R. Halmosi, E. Szabados, L. Czopf, T. Kálai, K. Hideg, B. Sümegi, K. Tóth, The role of Akt and mitogen-activated protein kinase systems in the protective effect of poly(ADP-ribose) polymerase inhibition in Langendorff perfused and in isoproterenol-damaged rat hearts, J. Pharmacol. Exp. Ther. 315 (2005) 273–282, https://doi.org/10.1124/jpet.105.088336.

[19] A. Palfi, A. Toth, K. Hanto, P. Deres, E. Szabados, Z. Szereday, G. Kulcsar, T. Kalai, K. Hideg, F.G. Jr, B. Sumegi, K. Toth, R. Halmosi, PARP inhibition prevents postinfarction myocardial remodeling and heart failure via the protein kinase C/glycogen synthase kinase-3β pathway, J. Mol. Cell. Cardiol. 41 (2006) 149–159, https://doi.org/10.1016/j.yjmcc.2006.03.427.

[20] E. Bartha, G.N. Kiss, E. Kalman, G. Kulcsár, T. Kálai, K. Hideg, T. Habon, B. Sumegi, K. Toth, R. Halmosi, Effect of L-2286, a poly(ADP-ribose)polymerase inhibitor and enalapril on myocardial remodeling and heart failure, J. Cardiovasc. Pharmacol. 52 (2008) 253–261, https://doi.org/10.1097/FJC.0b013e3181855cef.

[21] E. Bartha, I. Solti, L. Kereskai, J. Lantos, E. Plozer, K. Magyar, E. Szabados, T. Kálai, K. Hideg, R. Halmosi, B. Sumegi, K. Toth, PARP inhibition delays transition of

hypertensive cardiopathy to heart failure in spontaneously hypertensive rats, Cardiovasc. Res. 83 (2009) 501–510, https://doi.org/10.1093/cvr/cvp144.
[22] E. Bartha, I. Solti, A. Szabo, G. Olah, K. Magyar, E. Szabados, T. Kalai, K. Hideg, K. Toth, D. Gero, C. Szabo, B. Sumegi, R. Halmosi, Regulation of kinase cascade activation and heat shock protein expression by poly(ADP-ribose) polymerase inhibition in doxorubicin-induced heart failure, J. Cardiovasc. Pharmacol. 58 (2011) 380–391, https://doi.org/10.1097/FJC.0b013e318225c21e.
[23] L. Deres, E. Bartha, A. Palfi, K. Eros, A. Riba, J. Lantos, T. Kalai, K. Hideg, B. Sumegi, F. Gallyas, K. Toth, R. Halmosi, PARP-inhibitor treatment prevents hypertension induced cardiac remodeling by favorable modulation of heat shock proteins, Akt-1/GSK-3β and several PKC isoforms, PLoS One 9 (2014), https://doi.org/10.1371/journal.pone.0102148.
[24] K. Magyar, L. Deres, K. Eros, K. Bruszt, L. Seress, J. Hamar, K. Hideg, A. Balogh, F. Gallyas, B. Sumegi, K. Toth, R. Halmosi, A quinazoline-derivative compound with PARP inhibitory effect suppresses hypertension-induced vascular alterations in spontaneously hypertensive rats, Biochim. Biophys. Acta (BBA) - Mol. Basis Dis. 1842 (2014) 935–944, https://doi.org/10.1016/j.bbadis.2014.03.008.
[25] R. Halmosi, L. Deres, R. Gal, K. Eros, B. Sumegi, K. Toth, PARP inhibition and postinfarction myocardial remodeling, Int. J. Cardiol. 217 (2016) S52–S59, https://doi.org/10.1016/j.ijcard.2016.06.223.
[26] K. Eros, K. Magyar, L. Deres, A. Skazel, A. Riba, Z. Vamos, T. Kalai, F. Gallyas, B. Sumegi, K. Toth, R. Halmosi, Chronic PARP-1 inhibition reduces carotid vessel remodeling and oxidative damage of the dorsal hippocampus in spontaneously hypertensive rats, PLoS One 12 (2017), https://doi.org/10.1371/journal.pone.0174401.
[27] L. Deres, K. Eros, O. Horvath, N. Bencze, C. Cseko, S. Farkas, T. Habon, K. Toth, R. Halmosi, The effects of bradykinin B1 receptor antagonism on the myocardial and vascular consequences of hypertension in SHR rats, Front. Physiol. 10 (2019), https://doi.org/10.3389/fphys.2019.00624.
[28] J.G. Edwards, Quantification of mitochondrial DNA (mtDNA) damage and error rates by real-time QPCR, Mitochondrion 9 (2009) 31–35, https://doi.org/10.1016/j.mito.2008.11.004.
[29] S.A. Doggrell, L. Brown, Rat models of hypertension, cardiac hypertrophy and failure, Cardiovasc. Res. 39 (1998) 89–105, https://doi.org/10.1016/S0008-6363(98)00076-5.
[30] M. Kokubo, A. Uemura, T. Matsubara, T. Murohara, Noninvasive evaluation of the time course of change in cardiac function in spontaneously hypertensive rats by echocardiography, Hypertens. Res. 28 (2005) 601–609, https://doi.org/10.1291/hypres.28.601.
[31] V. Chan, A. Fenning, S.P. Levick, D. Loch, P. Chunduri, A. Iyer, Y.L. Teo, A. Hoey, K. Wilson, D. Burstow, L. Brown, Cardiovascular changes during maturation and ageing in male and female spontaneously hypertensive rats, J. Cardiovasc. Pharmacol. 57 (2011) 469–478, https://doi.org/10.1097/FJC.0b013e3182102c3b.
[32] C. Magnussen, S. Blankenberg, Biomarkers for heart failure: small molecules with high clinical relevance, J. Intern. Med. 283 (2018) 530–543, https://doi.org/10.1111/joim.12756.
[33] N.A. Berger, V.C. Besson, A.H. Boulares, A. Bürkle, A. Chiarugi, R.S. Clark, N. J. Curtin, S. Cuzzocrea, T.M. Dawson, V.L. Dawson, G. Haskó, L. Liaudet, F. Moroni, P. Pacher, P. Radermacher, A.L. Salzman, S.H. Snyder, F.G. Soriano, R. P. Strosznajder, B. Sümegi, R.A. Swanson, C. Szabo, Opportunities for the repurposing of PARP inhibitors for the therapy of non-oncological diseases, Br. J. Pharmacol. 175 (2018) 192–222, https://doi.org/10.1111/bph.13748.
[34] A. Tapodi, Z. Bognar, C. Szabo, F. Gallyas, B. Sumegi, E. Hocsak, PARP inhibition induces Akt-mediated cytoprotective effects through the formation of a mitochondria-targeted phospho-ATM-NEMO-Akt-mTOR signalosome, Biochem. Pharmacol. 162 (2019) 98–108, https://doi.org/10.1016/j.bcp.2018.10.005.
[35] F. Gallyas Jr, B. Sumegi, Mitochondrial protection by PARP inhibition, Int. J. Mol. Sci. 21 (2020) 2767, https://doi.org/10.3390/ijms21082767.
[36] S. Miyamoto, A.N. Murphy, J.H. Brown, Akt mediated mitochondrial protection in the heart, J. Bioenerg. Biomembr. 41 (2009) 169–180, https://doi.org/10.1007/s10863-009-9205-y.
[37] B. Racz, K. Hanto, A. Tapodi, I. Solti, N. Kalman, P. Jakus, K. Kovacs, B. Debreceni, F. Gallyas, B. Sumegi, Regulation of MKP-1 expression and MAPK activation by PARP-1 in oxidative stress: a new mechanism for the cytoplasmic effect of PARP-1 activation, Free Radic. Biol. Med. 49 (2010) 1978–1988, https://doi.org/10.1016/j.freeradbiomed.2010.09.026.
[38] Q. Jin, R. Li, N. Hu, T. Xin, P. Zhu, S. Hu, S. Ma, H. Zhu, J. Ren, H. Zhou, DUSP1 alleviates cardiac ischemia/reperfusion injury by suppressing the Mff-required mitochondrial fission and Bnip3-related mitophagy via the JNK pathways, Redox Biol. 14 (2017) 576–587, https://doi.org/10.1016/j.redox.2017.11.004.
[39] R. Halmosi, Z. Berente, E. Osz, K. Toth, P. Literati-Nagy, B. Sumegi, Effect of poly (ADP-ribose) polymerase inhibitors on the ischemia-reperfusion-induced oxidative cell damage and mitochondrial metabolism in Langendorff heart perfusion system, Mol. Pharmacol. 59 (2001) 1497–1505, https://doi.org/10.1124/mol.59.6.1497.
[40] B.N. Whitley, E.A. Engelhart, S. Hoppins, Mitochondrial dynamics and their potential as a therapeutic target, Mitochondrion 49 (2019) 269–283, https://doi.org/10.1016/j.mito.2019.06.002.
[41] C.-R. Chang, C. Blackstone, Dynamic regulation of mitochondrial fission through modification of the dynamin-related protein Drp1, Ann. N. Y. Acad. Sci. 1201 (2010) 34–39, https://doi.org/10.1111/j.1749-6632.2010.05629.x.
[42] A.J. Roe, X. Qi, Drp1 phosphorylation by MAPK1 causes mitochondrial dysfunction in cell culture model of Huntington's disease, Biochem. Biophys. Res. Commun. 496 (2018) 706–711, https://doi.org/10.1016/j.bbrc.2018.01.114.
[43] B. Westermann, Bioenergetic role of mitochondrial fusion and fission, Biochim. Biophys. Acta BBA - Bioenerg. 1817 (2012) 1833–1838, https://doi.org/10.1016/j.bbabio.2012.02.033.
[44] R. Das, O. Chakrabarti, Mitochondrial hyperfusion: a friend or a foe, Biochem. Soc. Trans. 48 (2020) 631–644, https://doi.org/10.1042/BST20190987.
[45] N. Nissanka, C.T. Moraes, Mitochondrial DNA damage and reactive oxygen species in neurodegenerative disease, FEBS Lett. 592 (2018) 728–742, https://doi.org/10.1002/1873-3468.12956.
[46] A. Signes, E. Fernandez-Vizarra, Assembly of mammalian oxidative phosphorylation complexes I–V and supercomplexes, Essays Biochem. 62 (2018) 255–270, https://doi.org/10.1042/EBC20170098.
[47] R.C. Scarpulla, Metabolic control of mitochondrial biogenesis through the PGC-1 family regulatory network, Biochim. Biophys. Acta 1813 (2011) 1269–1278, https://doi.org/10.1016/j.bbamcr.2010.09.019.
[48] P.J. Fernandez-Marcos, J. Auwerx, Regulation of PGC-1α, a nodal regulator of mitochondrial biogenesis1234, Am. J. Clin. Nutr. 93 (2011), 884S-890S, https://doi.org/10.3945/ajcn.110.001917.
[49] T. Ichiki, Role of cAMP response element binding protein in cardiovascular remodeling: good, bad, or both? Arterioscler. Thromb. Vasc. Biol. 26 (2006) 449–455, https://doi.org/10.1161/01.ATV.0000196747.79349.d1.
[50] S. Rius-Pérez, I. Torres-Cuevas, I. Millán, Á.L. Ortega, S. Pérez, PGC-1α, inflammation, and oxidative stress: an integrative view in metabolism, Oxidative Med. Cell. Longev. 2020 (2020), e1452696, https://doi.org/10.1155/2020/1452696.